An Atlas of Oceanic Internal Solitary Waves (May 2002)   **Oceanic Internal Waves and Solitons**
by Global Ocean Associates
Prepared for Office of Naval Research – Code 322 PO

Oceanic Internal Waves and Solitons
by John R. Apel[*]

1. Introduction

Internal waves (IWs) are, as their name implies, waves that travel within the interior of a fluid. Such waves are most familiar as oscillations visible in a two-layer fluid contained in a clear plastic box often sold in novelty stores. In the box, two immiscible and differently colored fluids fill the entire volume; when tilted or otherwise disturbed, a slow large amplitude wave is observed to propagate along the interface between the fluids. This is the internal wave and while it has its maximum amplitude at the interface, its displacements are zero at the top and bottom. It owes its existence to the stratified density structure of the two fluids, with a very sharp density change occurring along the interface and with the properties that the smaller the density contrast, the lower the wave frequency, and the slower the propagation speed. [*Apel, 1987*]

Similar modes exist within the geophysical fluids of the atmosphere and ocean. Solar radiation is absorbed in the near surface layers, resulting in warmer water and lower density in that region and leading to a stratified fluid. Upper ocean temperature and salinity gradients are relatively sharp under most conditions and any excitation or disturbance of the pycnocline (a zone within which seawater density changes maximally) will tend to propagate away from the region of generation as an internal wave. [*Apel, 1987*]

Internal solitary waves are important for many practical reasons. They are ubiquitous wherever strong tides and stratification occur in the neighborhood of irregular topography. As such, they are often prominent features seen in optical and radar satellite imagery of coastal waters. They can propagate over several hundred kilometers and transport both mass and momentum. Indeed, an early motivation for studying them was the unexpectedly large stresses they imposed on offshore oil-drilling rigs. They are often associated with a net change in stratification in which form they constitute travelling internal undular bores. Their propagation carries with it considerable velocity shear that can lead to turbulence and mixing. The mixing often introduces bottom nutrients into the water column, thereby fertilizing the local region and modifying the biology therein.

This Second Edition of the *Atlas of Oceanic Internal Solitary Waves* contains over 300 examples from some 54 regions of the world where oceanic internal wave manifestations have been observed (Figure 1). Most of the sites have been found through surface signatures of an internal soliton group within remote sensing images. In a few cases, however, it has been in-situ data that has shown the existence of such waves.

The case studies include information on the spatial distributions of the solitons, speculating on sources, characteristics (wavelengths, and speeds) and any available modeling or analyses efforts. Image types include: high-resolution satellite from synthetic aperture radar (SAR), scanning radiometers, photographs from manned space flights, and photographs from incidental aircraft flights. Each of the images demonstrates surface signatures of coherent; hence, distinctly recognizable internal waves. In each instance within a case study, the data usually includes an image that inspired the initiation of the study, some supporting data and ancillary information, an analysis, and/or interpretations in terms of solitary wave models. While

---

An Atlas of Oceanic Internal Solitary Waves (May 2002)   **Oceanic Internal Waves and Solitons**
by Global Ocean Associates
Prepared for Office of Naval Research – Code 322 PO

not advocating any particular model of internal solitary waves, included are Korteweg-de Vries environmental parameters (α, γ, and c_0) that have been evaluated from the available data and useful in most any theoretical effort. Supporting data include: bathymetric maps, temperature/salinity or density profiles for the approximate place and time of the image acquisition (usually gleaned from data archives); and such current, or temperature-time series as may be available.

The locales range over most of the oceans and seas of the world, although they are dependent upon the seasons and the myriad of tidal cycles, as well. The Atlas is intended to show the ubiquitous nature of this phenomenon. The internal waves appear wherever the combination of stratified waters, currents, and bathymetry is correct; and the recurrence of the signatures suggests that this combination occurs frequently within the seas.

2. The Nature of Solitary Waves

The particular type of IW most often seen is termed a *solitary wave* or *soliton.* Solitary waves are a class of nonsinusoidal, nonlinear, more-or-less isolated waves of complex shape that occur frequently in nature. These waves maintain their coherence, and hence visibility, through nonlinear hydrodynamics and appear as long, quasilinear stripes in imagery. The internal wave signatures are made visible by wave/current interactions; wherein the near-surface current associated with the internal wave locally modulates the surface wave height spectrum. The primary modulations typically occur at wavelengths ranging from a few meters down to perhaps 10 to 50 cm, but secondary interactions further transport surface wave energy down to sub-centimeter scales. Thus, a roughening of the short-wave portion of the surface wave spectrum takes place in regions of internal wave phase where the currents are convergent. At a distance of one-half of an internal waves phase to the rear, the sea surface has been swept relatively clean of surface wave energy, and the ocean in this phase region is very flat.

On the face of it, a "solitary wave" is a contradiction in terms because a wave is usually considered a repeating, oscillating motion or force. However, this terminology is deeply embedded in the scientific literature, along with a less well known, but more discrete term, sometimes referred to as a *soliton*. The internal solitons existing in the ocean are usually composed of several oscillations confined to a limited region of space. For these, the term "solitary wave packets" seems more appropriate and so shall be referred to in the main. However, the other terms will also be used from time to time; hopefully, with no resulting confusion.

3. Observations

The earliest recognition of internal wave phenomena appears to have been by J. Scott Russell [*1838, 1844*] who reported on the formation of a single, unchanging hump or mound in the shallow water of Scottish canal, generated when a towed barge was brought to a sharp halt in the canal. Russell followed the wave for several miles on horseback until he lost it in the windings of the canal. Later Korteweg and deVries [*1895*] derived some of the interesting mathematical properties of such a wave and produced their now-famous soliton solutions. The attention given to solitary waves since has been in the main due to their strange and interesting mathematical characteristics. Recently, however, it has been the recognition of their wide-spread occurrence in the ocean that has spurred geophysically oriented investigations, not only into the internal hydrodynamics but on their attendant impacts on surface wave spectra, air-sea interaction, remote sensing science, shallow-water acoustics, and coastal mixed-layer dynamics.

An Atlas of Oceanic Internal Solitary Waves (May 2002)   **Oceanic Internal Waves and Solitons**
by Global Ocean Associates
Prepared for Office of Naval Research – Code 322 PO

Reports of what are almost certainly surface manifestations of oceanic internal solitary waves are centuries, if not millennia old, but their scientific study is more recent. It has been known for over 150 years that in the island archipelagos of the Far East, there are occasionally seen on the surface of the sea long, isolated stripes of highly agitated features that are defined by audibly breaking waves and white water [*Wallace, 1869*]. These features propagate past vessels at speeds that are at times in excess of two knots; they are not usually associated with any nearby bottom feature to which one might attribute their origin, but are indeed often seen in quite deep water. In the nautical literature and charts, they are sometimes identified as "tide rips". In Arctic and sub-Arctic regions, especially near the mouths of fjords or rivers flowing into the sea, analogous waves of lower energy are known, dating back perhaps even to the Roman reports of "sticky water," but certainly a recognized phenomenon – dead water – since Viking times [*Ekman, 1904*].

In the 1950's and '60's, during in-situ measurements of internal waves, it was noted that they were accompanied by surface "slicks" [*Ewing, 1950; Shand, 1953*]. It was thought that these slicks were due to natural surfactants that dampened the ultragravity and capillary waves, constituting small-scale surface roughness. In certain cases, however, it was noted that there appeared to be regions of enhanced, (rather than reduced) surface roughness [*Gargett and Hughes, 1972*]. Debate went on as to the cause and effect until theoretical analyses showed that regions of both enhanced and reduced roughness accompanied the waves, with the roughened region generally leading the smoother one because of modulations by the underlying internal wave currents. The dominance of one signature type over the other depended on the wind speed and the strength of the internal wave currents near the surface.

With the advent of aircraft and satellite imaging sensors, a more Olympian perspective became available from which to view the surface signatures. Apel et al. *[1975a]* reported the existence of solitons in the New York Bight based on ERTS (Earth Resource Technology Satellite) imagery collected in August 1972 May 1973 and July 1973. The visible wave packets demonstrate the prototypical multiple oscillations, variable wavelengths and crest lengths; and as later documented, reduced amplitudes toward the rear of the packet. The analyses laid down the basic characteristics of the internal waves in this area of the U.S. East Coast. The wide-ranging data from satellites soon showed analogous signals to exist at many locales around the world. While these often differed among themselves in scale or in detail, at many locations, the wave packets had strong topographical similarities to each other. With the assistance of in-situ experiments in the New York Bight, the Massachusetts Bay, [*Halpern, 1970, 1971; Haury et al., 1979*] and in the Strait of Georgia [*Hughes and Gower, 1983*], the internal wave interpretation of these surface signatures became solidified.

At approximately the same time, a theoretical understanding of the effects of the wave currents on the surface wave spectrum grew, allowing more accurate and well-founded interpretations of the underlying internal wave displacements to be made from the overhead images. It was realized that the quantity being sensed in the imagery was more nearly the internal wave surface current gradients rather than the surface currents themselves [*Alpers* 1985]. The subsurface data showed that these waves had highly non-sinusoidal waveforms, at times even approaching those expected of a train of isolated pulses moving at their own individual speeds. An interpretation in terms of solitary wave theory arose with the applications and extensions of the Korteweg–de Vries formulations having proven to be quite adept at describing the wave characteristics quantitatively.

An Atlas of Oceanic Internal Solitary Waves (May 2002)   **Oceanic Internal Waves and Solitons**
by Global Ocean Associates
Prepared for Office of Naval Research – Code 322 PO

3.1 Global Occurrences

The remotely sensed images acquired during the quarter-century since the first glimpses of oceanic solitons were obtained from the ERTS/Landsat-1 spacecraft [*Apel et al., 1975a, 1975b; Sawyer and Apel, 1976*] have allowed the construction of global maps of their occurrence. Figure 1 shows the locations of solitons observed around the world with a variety of remote and in-situ sensors. The majority of these sensors are synthetic aperture radars operated by the United States, Canada, the European Space Agency, the USSR/Russia and Japan. Indeed, the SAR is the premier sensor for such phenomena, because of its sensitivity to small surface roughness changes at ocean surface wavelengths of the order of the radar wavelength, as well as its independence of cloud cover and solar illumination. In addition, it is a quantitative instrument because of control over such factors as frequency, phase, polarization, incidence angle, power, and swath width, all of which are important in the observation of oceanic phenomena

As the global maps show, solitary internal waves are widespread. If the theories of their generation and propagation are even approximately correct, then they should occur wherever the combination of stratification, bathymetry, and current flow conspire to give the needed conditions. It is apparent that these conditions happen frequently in coastal regions, especially during the summer months. Under conditions of summertime stratification, they even extend to sub-Arctic regions such as the coasts of Labrador [*Fu and Holt, 1982*], northern Norway, and the Barents Sea and the Antarctic in the Weddell Sea [*Levine et al., 1997*].

Nevertheless, there are interesting and important exceptions, such as the apparent solitary waves observed near the Mid-Atlantic Ridge north of the Azores [*Apel, 1987*], and in packets seen with shipboard acoustic Doppler current profilers (ADCPs) northeast of the Bismarck–Solomon Islands chain in the open South Pacific [*Pinkel et al., 1997*]. The Mid-Atlantic waves could be due to the Gulf Stream extension (pycnocline depths near 600 m) flowing over the Ridge (bottom depths near 900 m), and the Pacific Island solitons were probably generated near one of the inter–island sills in the region. However, there is a dearth of open-ocean SAR imagery, so that it is difficult to say how frequently deep-water solitons occur.

4. A Descriptive Canonical Picture

From the body of work addressing soliton characteristics [*Apel and Gonzales, 1984; Apel et al., 1985; Liu et al., 1985*], there has emerged a canonical picture of oceanic internal solitons and their generation, propagation, and dissipation. While any internal motions that are energetically possible can (and do) occur in the sea, a very large percentage of the examples at hand display the approximate attributes exhibited by the proposed canonical model. The mathematical description to be presented produces the dominant wave characteristics derived from numerous observations, with the major exceptions being those having somewhat pathological initial or final states. Only multiple observations can decide on whether the canonical model has the needed degree of verisimilitude.

In-situ observations of internal solitons can be made using almost any ocean instrumentation capable of recording current, density, displacement of planktonic layers, or similar quantities. Because they are coherent processes, the waves can be recognized in photographs of the sea surface, in multispectral radiometer images, in real and synthetic aperture radar images, and in vertically viewing echo-soundings made in the water. Even the eye at sea level can detect the induced surface-wave changes as rough and smooth regions. However, it has been remote sensing, both satellite radar and optical, with their Olympian view that has brought

4

An Atlas of Oceanic Internal Solitary Waves (May 2002)   **Oceanic Internal Waves and Solitons**
by Global Ocean Associates
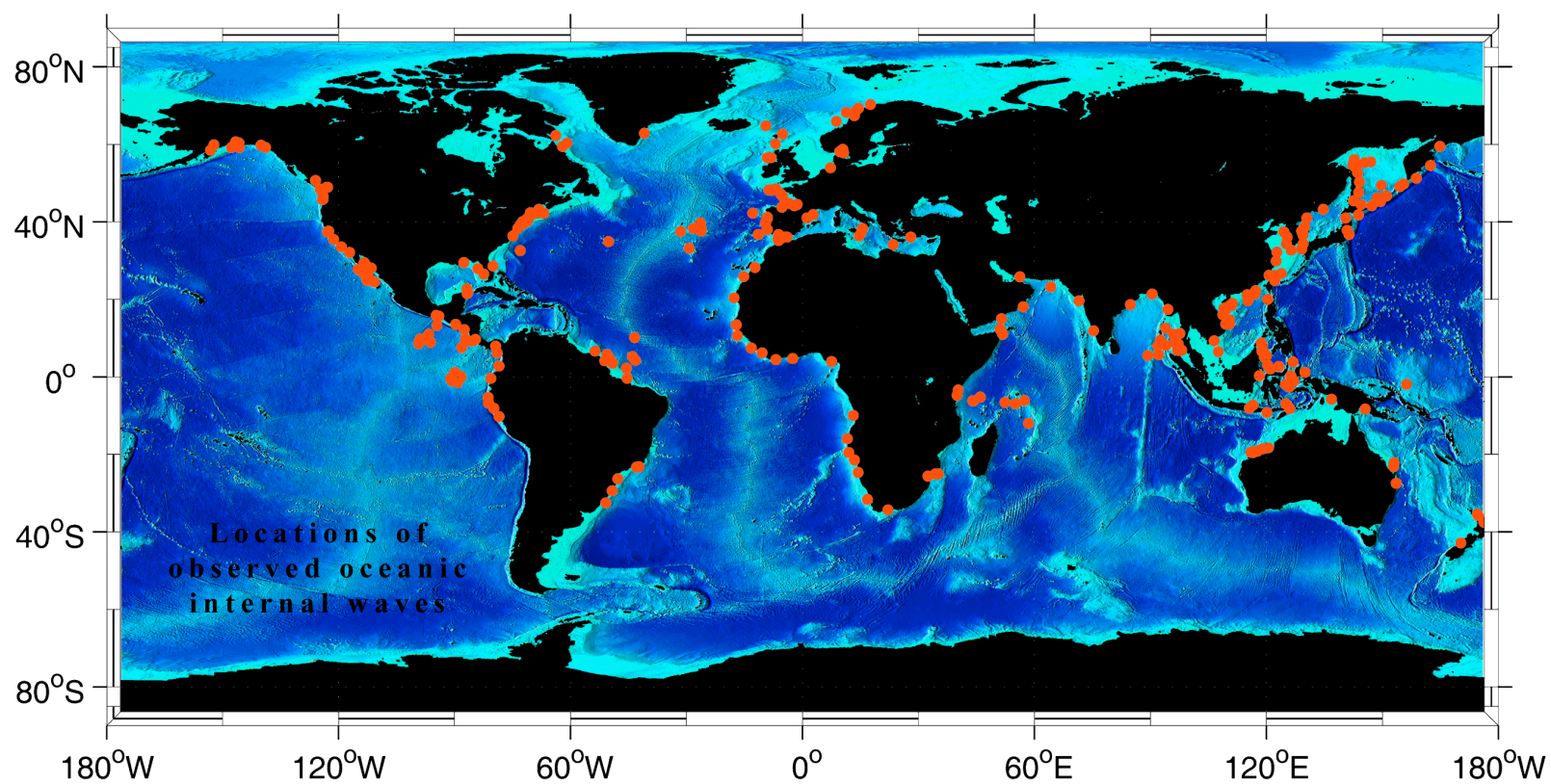Prepared for Office of Naval Research – Code 322 PO

Figure 1. Locations of internal wave imagery and data presented in the Second Edition of the *Atlas of Oceanic Internal Solitary Waves*. The vast majority are satellite images. Lack of open-ocean sites reflects paucity of data there.
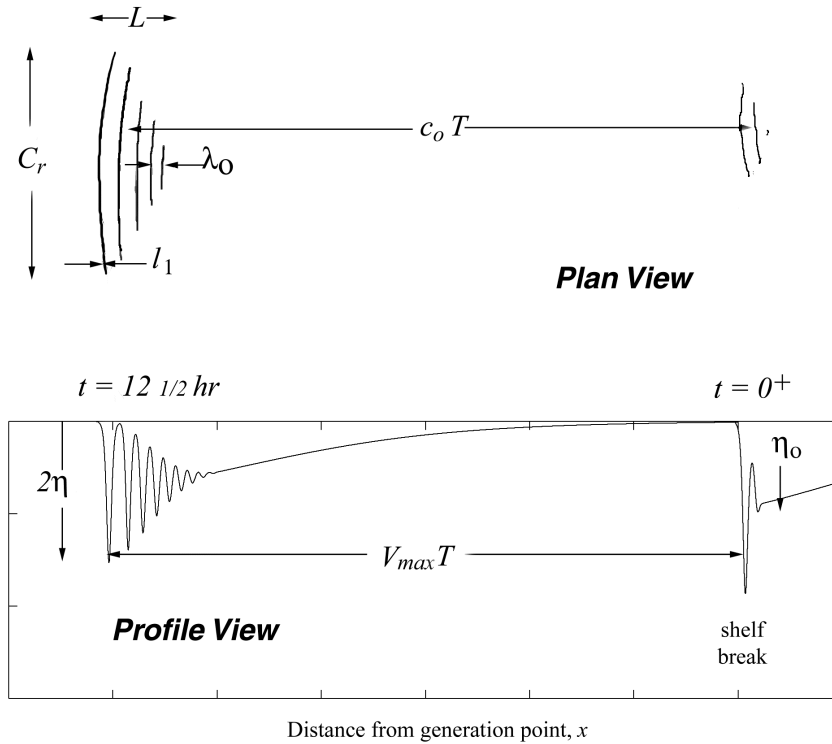
An Atlas of Oceanic Internal Solitary Waves (May 2002)   **Oceanic Internal Waves and Solitons**
by Global Ocean Associates
Prepared for Office of Naval Research – Code 322 PO

$\leftarrow L \rightarrow$

$c_o T$

C_r

λ_O

l_1

Plan View

$t = 12 \, 1/2 \, hr$ $t = 0^+$

2η

η_o

$V_{max} T$

Profile View   shelf
                                                         break

Distance from generation point, x

Figure 2: Schematic of tidally generated solitons on the continental shelf. V_{max} T is
the internal tidal wavelength; c_0T is distance between packet centroids.

Table 1.1. Typical scales for continental shelf solitons

Characteristic	Symbol	Scale
Packet Length	L (km)	1 – 10
Amplitude Factor	$2\boldsymbol{h}_0$(m)	-15
Upper Layer Depth	h_1(m)	20 – 35
Lower Layer Depth	h_2(m)	30 - 200
Long Wave Speed	c_0 (m s^{-1})	0.5 - 1.0
Maximum Wavelength	λ_{MAX} (m)	100 – 1000
Crest Length	C_r(km)	0 - 30
Internal Tidal Wavelength	$D = VT$ (km)	15 – 40
Characteristic Soliton Width	l_1(m)	100

6

An Atlas of Oceanic Internal Solitary Waves (May 2002)   **Oceanic Internal Waves and Solitons**
by Global Ocean Associates
Prepared for Office of Naval Research – Code 322 PO

about the realization of their widespread existence and provided the major impetus for their study. When enhanced by in-water measurements, it is possible to derive a more nearly three-dimensional picture of the waves, especially if aided by theoretical models of both the internal hydrodynamics and the surface wave–electromagnetic scattering processes. The description of the waves to follow is drawn from all these data sources.

4.1 Characteristics of Oceanic Solitary Internal Waves.

Internal solitons occur in stratified coastal waters as groups or packets of oscillations, with the number of cycles varying from a very few to a few dozen, depending on age and distance from generation point. They are usually produced by tidal currents flowing normal to the local bathymetry. Such processes are statistically quite reproducible, given the same season, the same phase of both the daily and fortnightly tides, and the bathymetry. Typical mid-latitude soliton packets form at the continental shelf break during the summer. The wave groups are generated approximately every 12 hours during the spring tide phase of the fortnightly (14-day) tidal current. At the neap tide phase, they are often absent. Seasonal and interannual variations in density and larger-scale currents also play a role.

A given wave packet is usually characterized by several dominant features. The individual oscillations are nonsinusoidal, with predominantly downward displacements (i.e., depression IWs); the amplitudes are rank-ordered, with the largest at the front of the packet and the smallest at its rear; the wavelengths and the crest lengths are also rank-ordered, with the longest waves again at the front of the group; and the number of individual oscillations within the packet increases as its age increases, with one new oscillation added per Brunt-Väisälä period. The Brunt-Väisälä or buoyancy period, describes the oscillation of a water parcel about its equilibrium depth, and is proportional to the square root of the change in density with depth. It is used as a parameter to express the strength of stratification in a fluid. Additionally, the maximum amplitude of the leading oscillations appears to be related to the magnitude of the downward displacement of the pycnocline during the ebb (offshore) tidal phase.

A schematic of these features is shown in Figure 2. Here are sketched two individual packets, the rightmost one having just been generated by offshore tidal flow at the shelf break within the last few hours, and the leftmost one being about 12 hours older and having been generated on the previous semidiurnal tide, and then propagating up onto the continental shelf on the order of 25 to 35 km from its formative point. This implies a phase speed of about 0.6 to 0.7 m/s, although what one means by "phase speed" needs a careful definition in terms of the theoretical models

Both a vertical section of displacement and a horizontal plan of the wave crests are sketched on Fig. 2. The vertical section shows that the displacements are mostly negative, and that the downward oscillations of the pycnocline are followed by a several-hour average depression of the density interface to the rear of the oscillatory region. A slow recovery of the pycnocline then takes place near the trailing edge of the undulation.

Typical scales for summertime continental shelf internal waves are given on Table 1. It should be emphasized that these characteristics are canonical, and any individual realization of a soliton packet can be expected to deviate from the ideal by significant factors.

Figure 3 shows a synthetic aperture radar image of four such continental shelf soliton packets northeast of the Hudson Canyon off New York, generated during the previous 50 hours of tidal action at the shelf break. Such data, together with in-situ observations, have gone into making up the canonical description of the wave field.

An Atlas of Oceanic Internal Solitary Waves (May 2002)   **Oceanic Internal Waves and Solitons**
by Global Ocean Associates
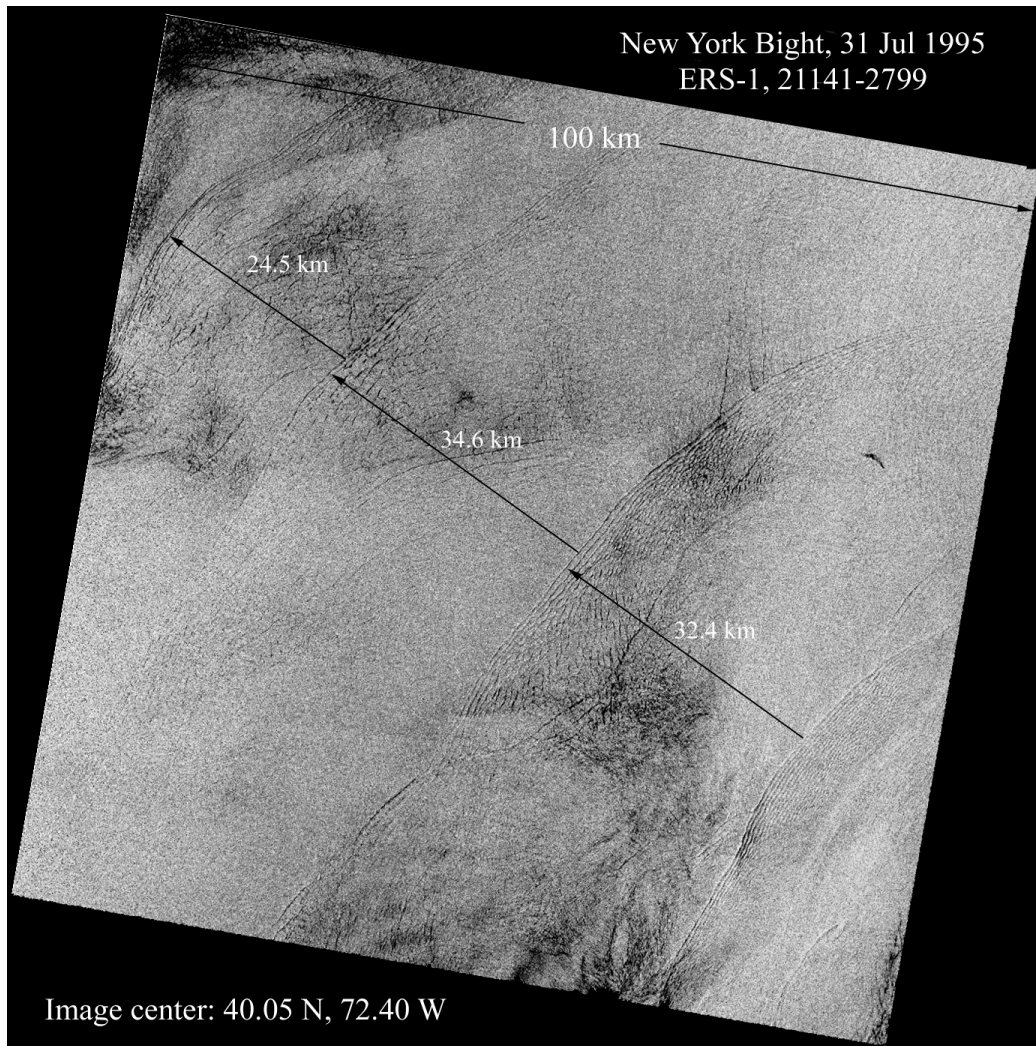Prepared for Office of Naval Research – Code 322 PO

Fig. 3. ERS-1 SAR image of the New York Bight taken on 31 July 1995. Image is approximately 100 km on a side. Four packets of tidally generated internal waves are visible north of the Hudson Canyon, which lies near the bottom center of the image. Distance between packets is set by 12 ½-h semidiurnal tidal period. ©Copyright European Space Agency, 1995

The proper view of these soliton groups is that they are oscillations of the leading edge of an undulatory internal bore, or nonlinear internal tide on the shelf. Both observational evidence and numerical models of nonlinear hydrodynamics under these conditions show that the linear deep-sea barotropic tides (tides characterized by a water height change throughout the water column) are transformed into nonlinear baroclinic tides (tides characterized by propagation of the tide as an internal wave propagating along the thermocline) as they move up on the shelf. Later, after several tidal cycles of their existence, dissipative forces reduce the nonlinearities to small values, so that near the shoreline, the tides are once again sinusoidal.

8

An Atlas of Oceanic Internal Solitary Waves (May 2002)   **Oceanic Internal Waves and Solitons**
by Global Ocean Associates
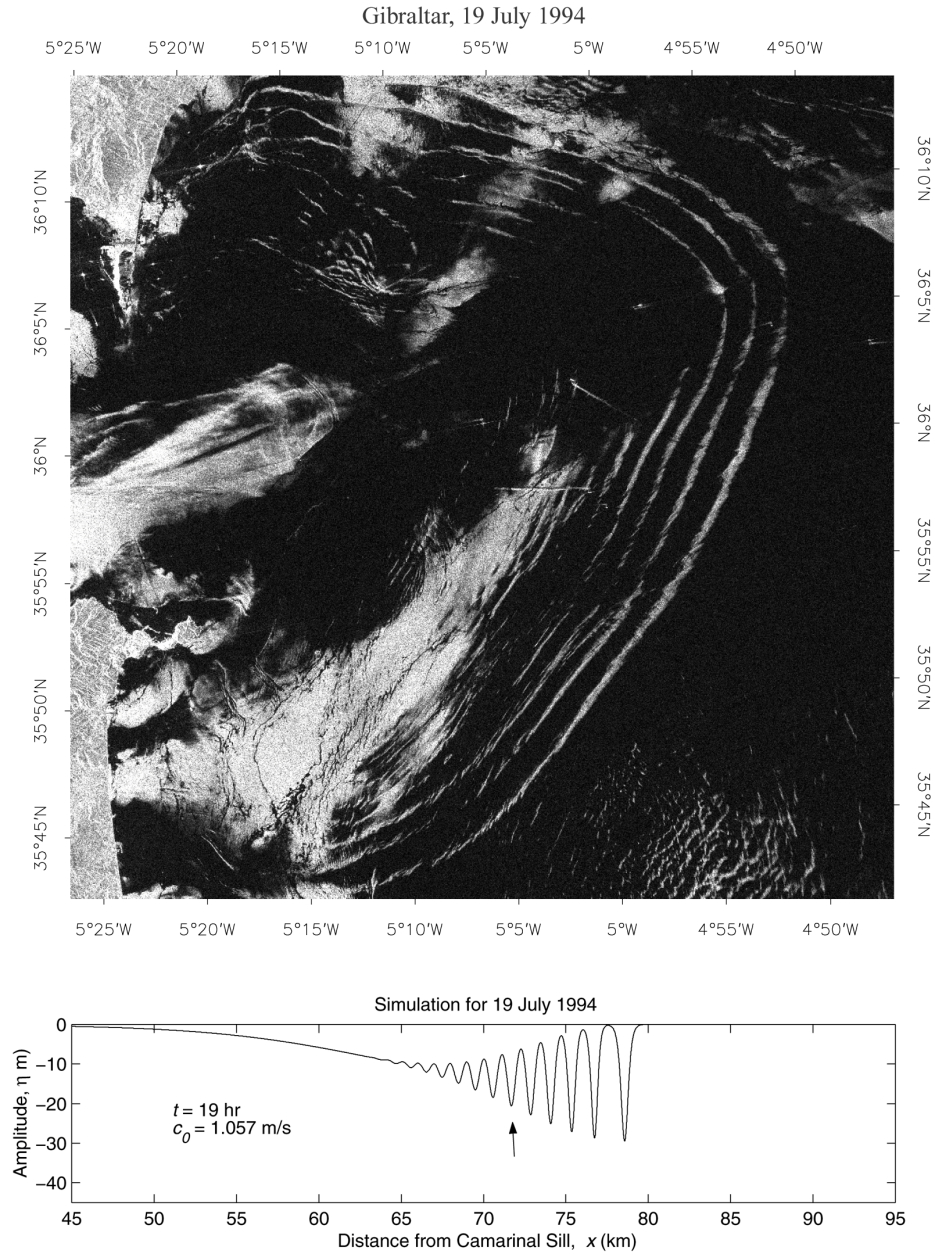Prepared for Office of Naval Research – Code 322 PO

Figure 4. (Upper) SAR image of Mediterranean just east of Strait of Gibraltar, showing a large packet of solitons propagating into the Alboran Sea. The generation region is near the Camarinal Sill. Dimensions 50 × 50 km. Image © European Space Agency, 1994. (Lower). Simulation of soliton packet using dnoidal model with historical observations of r(z) and U_0(z), and initial amplitude derived from Fig. 5.

An Atlas of Oceanic Internal Solitary Waves (May 2002)   **Oceanic Internal Waves and Solitons**
by Global Ocean Associates
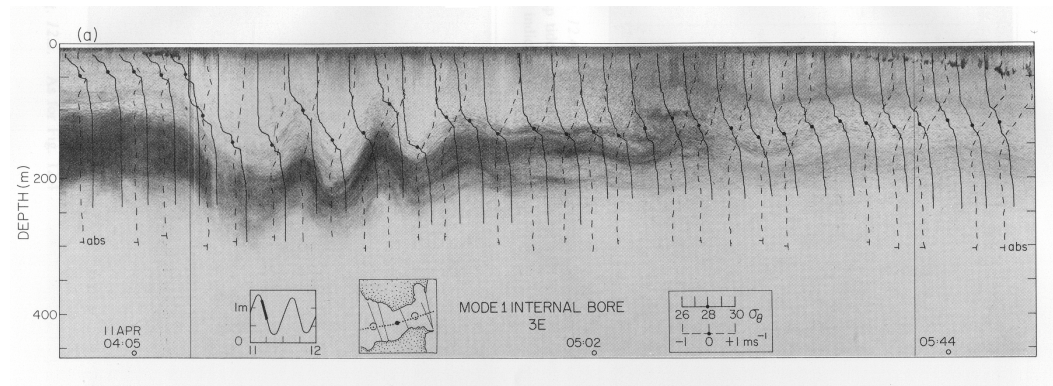Prepared for Office of Naval Research – Code 322 PO

Fig 5. Echo-sounder profile of large soliton packet in the center of Tarife Narrows in Gibraltar, taken in April 1986. The lead (leftmost) soliton shows considerable broadening, possibly due to higher-order nonlinearities at work there. Double amplitude $2h \cong$ 80-m. Solid vertical lines are densities from CTD casts, and dashed lines are relative east-west velocity profiles from ADCP's. [*Farmer and Armi; Armi and Farmer, 1988*]

Soliton packets are also generated by tidal flow over relatively shallow sills or banks. While the generation process is probably similar to that at the continental shelf break, the subsequent evolution of the individual packets can be considerably different.   Instead of encountering ever-decreasing water depths, the sill-formed soliton radiates into a deeper sea, and is less controlled by bathymetry (although depths continue to play a role as long as they are roughly less than the soliton wavelength). The restrictions in the Strait of Gibraltar, i.e. the Camarinal and Spartel Sills, are generation regions of great importance for the western Mediterranean and regularly produce solitons with amplitudes of 50 to 100 m and wavelengths of two to four km [*Farmer and Armi; Armi and Farmer, 1988*]. Similar situations occur in the Sulu Sea in the Philippines [*Apel and Holbrook, 1983; Apel et al., 1985; Liu et al., 1985*], the strait between Luzon and Taiwan [*Hsu and Liu, 2000a; Hsu and Liu, 2000b*], and the arcs of the Andaman and Nicobar Islands in the eastern Indian Ocean [*Apel, 1979; Osborne and Burch, 1980; Alpers et al., 1997*]. In the western tropical Pacific, the pycnocline depths are in excess of 100 m, and therefore, these sill regions are sources of intense internal solitons whose amplitudes can exceed 100 m and whose wavelengths can grow as great as 20 km.

Figure 4 shows a packet of solitons radiating eastward from the Strait of Gibraltar, having been formed by intense westward tidal flow across the Camarinal Sill several hours earlier [*Apel, 2000*]. The image is from the European Remote Sensing Satellite ERS-1; at the bottom is a simulation of the soliton displacement using the dnoidal model of Section 5.2.4. An echo-sounder profile from this region is shown on Fig. 5 [*Armi and Farmer, 1988; Farmer and Armi, 1988*]. Such packets reach at least 200 km into the western Mediterranean Sea and live for more than two days before decaying toward background levels [*Apel, 2000*]. Figure 6 illustrates an image of the Sulu Sea, obtained from the U.S. Defense Meteorological Satellite Program in 1973, showing five groups of solitons propagating over 500 km across the Sulu Sea between Mindanao and Palawan Island in the Philippines [*Apel et al., 1985; Liu et al., 1985*]. Such large waves are formed by intense (>3 m/s) tidal flow across a sill at the south end of the Sea, and have amplitudes in excess of 100 m.

10

An Atlas of Oceanic Internal Solitary Waves (May 2002)   **Oceanic Internal Waves and Solitons**
by Global Ocean Associates
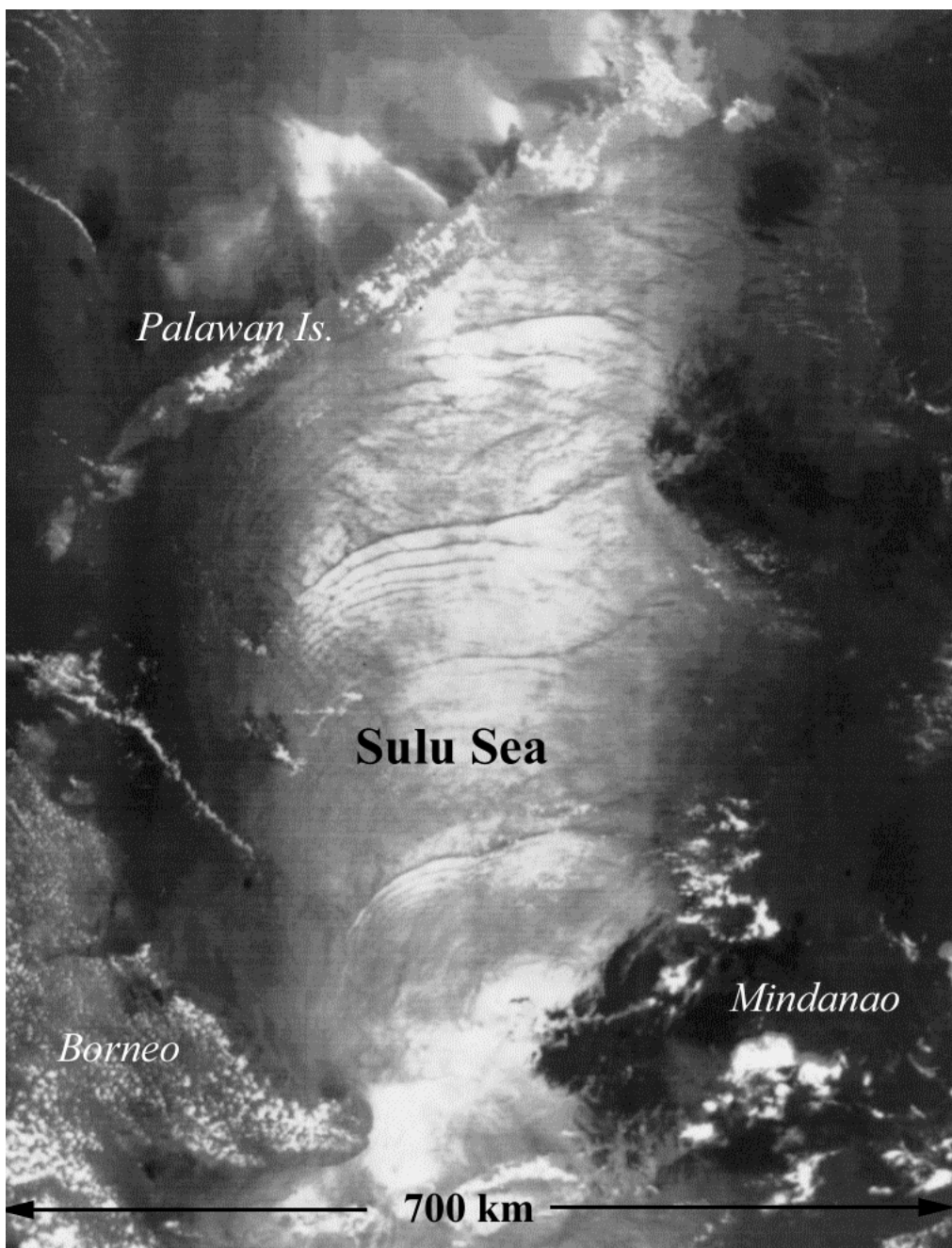Prepared for Office of Naval Research – Code 322 PO

Fig. 6. DMSP image of Sulu Sea, Philippine Islands, in April 1973, made in visible light. Solar reflection shows roughness modulations from five groups of large internal solitons generated at a small sill between Mindanao and Borneo. Amplitudes near 100 m, wavelengths between 2 and 20 km, phase speeds about 2 m/s. Figure courtesy of U.S. Air Force

An Atlas of Oceanic Internal Solitary Waves (May 2002)   **Oceanic Internal Waves and Solitons**
by Global Ocean Associates
Prepared for Office of Naval Research – Code 322 PO
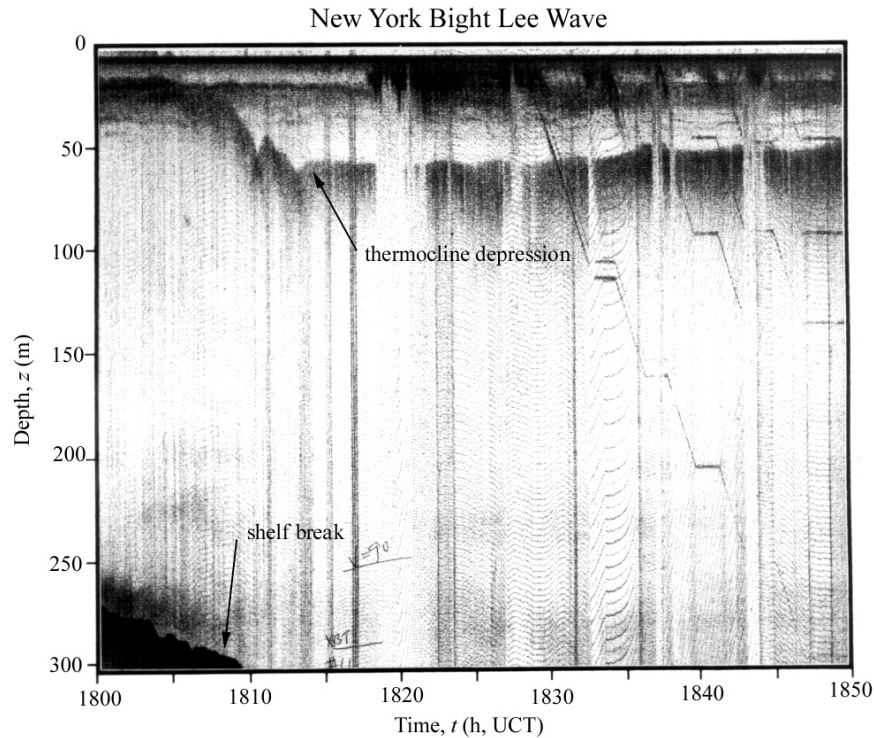
New York Bight Lee Wave

Fig. 7. Lee wave formation at the shelf break in the New York Bight, seen via 20-kHz echo-sounder. XBT and CTD casts confirm pycnocline depression. June 1976.

4.2 Generation Phase at the Continental Shelf Break and at Sills

There has not been much work on the generation phase of oceanic solitons, but such as there is suggests that during the phase of the barotropic tide when off-shelf or off-sill flow is occurring, a steep depression of the pycnocline develops on the deep-water side of the bathymetry. Figure 7 is an acoustic echo-sounder record from the New York Bight showing such a depression taking place just beyond the 200-m isobath. The plunging of the pycnocline near t =1810 UTC has a full amplitude, $2h_0 \approx$ -45 m, and there is some evidence that undulatory motion exists offshore of the break. One theory of generation suggests that the operative process is formation of a lee wave down-current of a sharp change of bathymetry [*Maxworthy, 1979; D. Farmer, personal communication, 2000*]. Figure 8, from Georges Bank/Gulf of Maine [*P. Wiebe and T. Stanton personal communication, 1999*] illustrates the lee-wave character even more clearly, via depression of biological scattering layers sampled with high-frequency echo-sounders. Similar steep depressions of the pycnocline have been observed on the outgoing tide at the Camarinal Sill just west of Gibraltar [*Armi and Farmer, 1988; Farmer and Armi, 1988; Wesson and Gregg, 1988*] and in Knight Inlet in western Canada [*Farmer and Armi, 1999; Farmer and Smith, 1980*]. Figure 9 shows observations of the evolution of the soliton packet made via CTD casts in the Strait of Gibraltar. The isopycnal, $\sigma_\theta = 28.0$ kg/m^3, plunges by over 100 m at
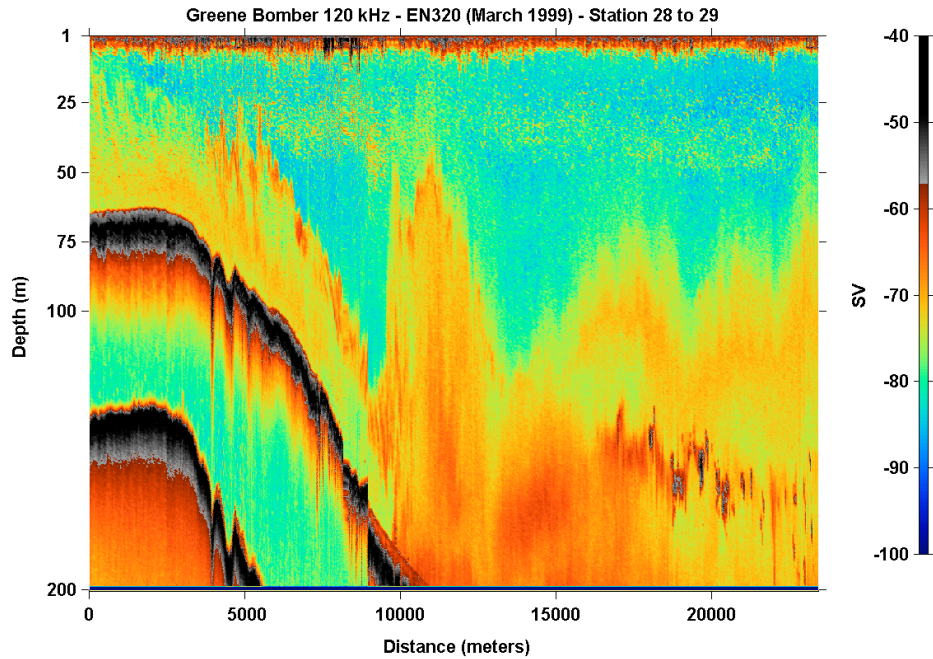
12

An Atlas of Oceanic Internal Solitary Waves (May 2002)   **Oceanic Internal Waves and Solitons**
by Global Ocean Associates
Prepared for Office of Naval Research – Code 322 PO

Fig. 8. Lee wave off north edge of Georges Bank (42.2°N, 66.9°W), viewed with 200 kHz echo-sounder. [Wiebe, P.H., J.D. Irish, R.C. Beardsley, and T.K. Stanton. 2000. Observations of internal solitary waves on Georges Bank. EOS 80(49):OS224 Poster
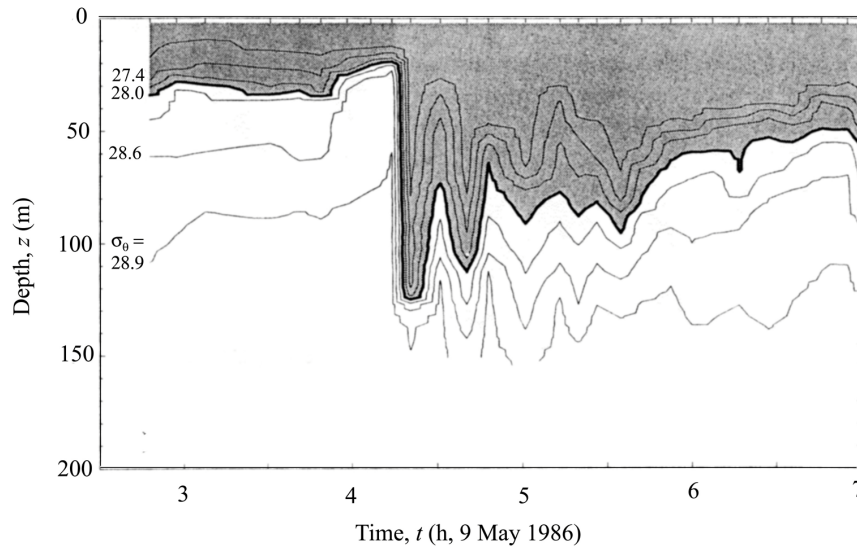

Fig. 9.   Pycnocline depression in Tarifa Narrows in the Strait of Gibraltar as observed via the Advanced Microstructure Profiler. Upper level currents ≤0.6 m/s to the east; lower level currents ≤0.4 m/s to the west. Figure courtesy of Wesson and Gregg (1988).

13

An Atlas of Oceanic Internal Solitary Waves (May 2002)   **Oceanic Internal Waves and Solitons**
by Global Ocean Associates
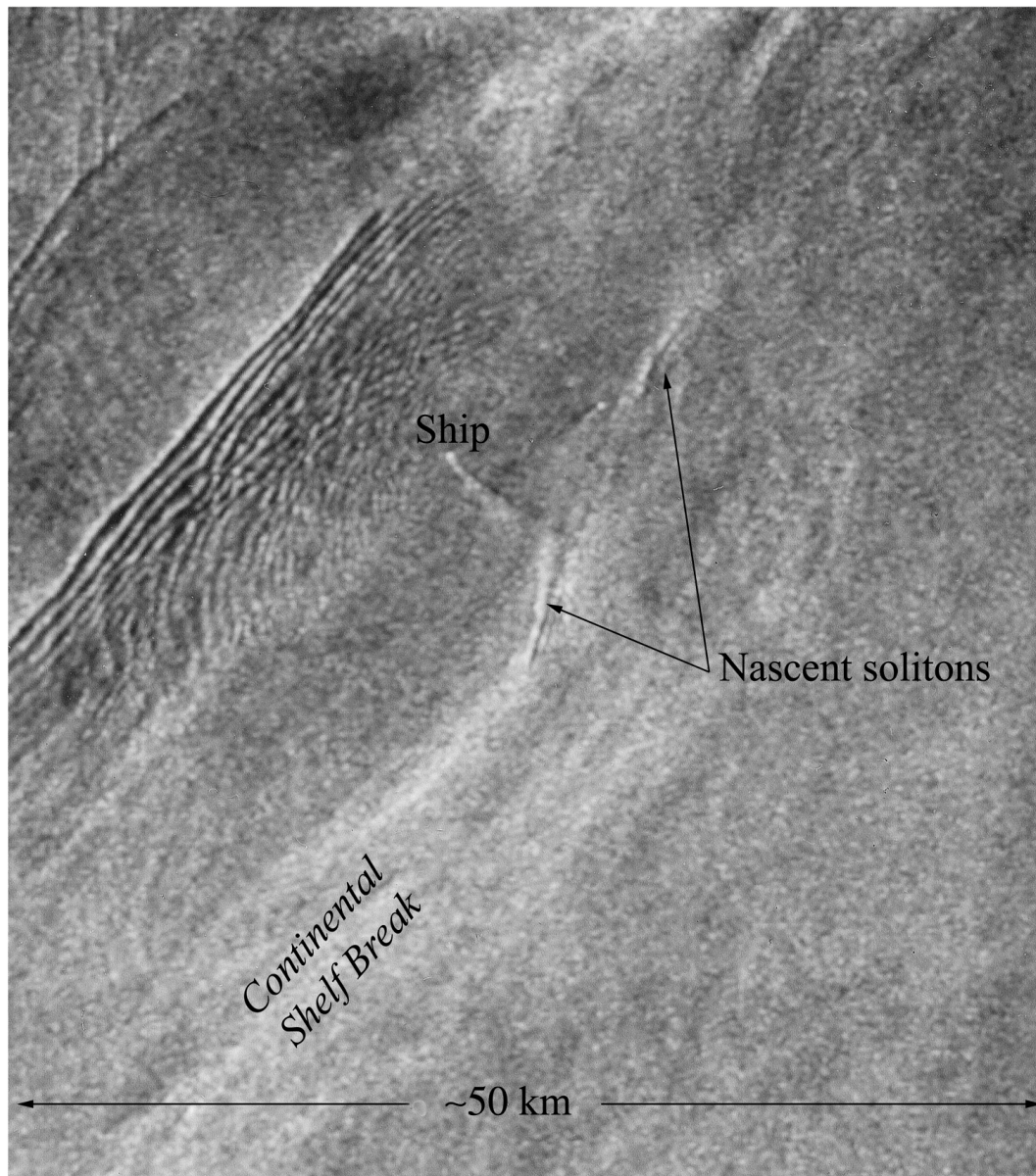Prepared for Office of Naval Research – Code 322 PO

Fig. 10. Solitons SW of Hudson Canyon in New York Bight, 18 Jul 1992. Nascent solitons are just being formed very near to the 200-m shelf break (cf. Fig. 4.) and will propagate toward the northwest. Original image © European Space Agency, 1992.

An Atlas of Oceanic Internal Solitary Waves (May 2002)
by Global Ocean Associates
Prepared for Office of Naval Research – Code 322 PO

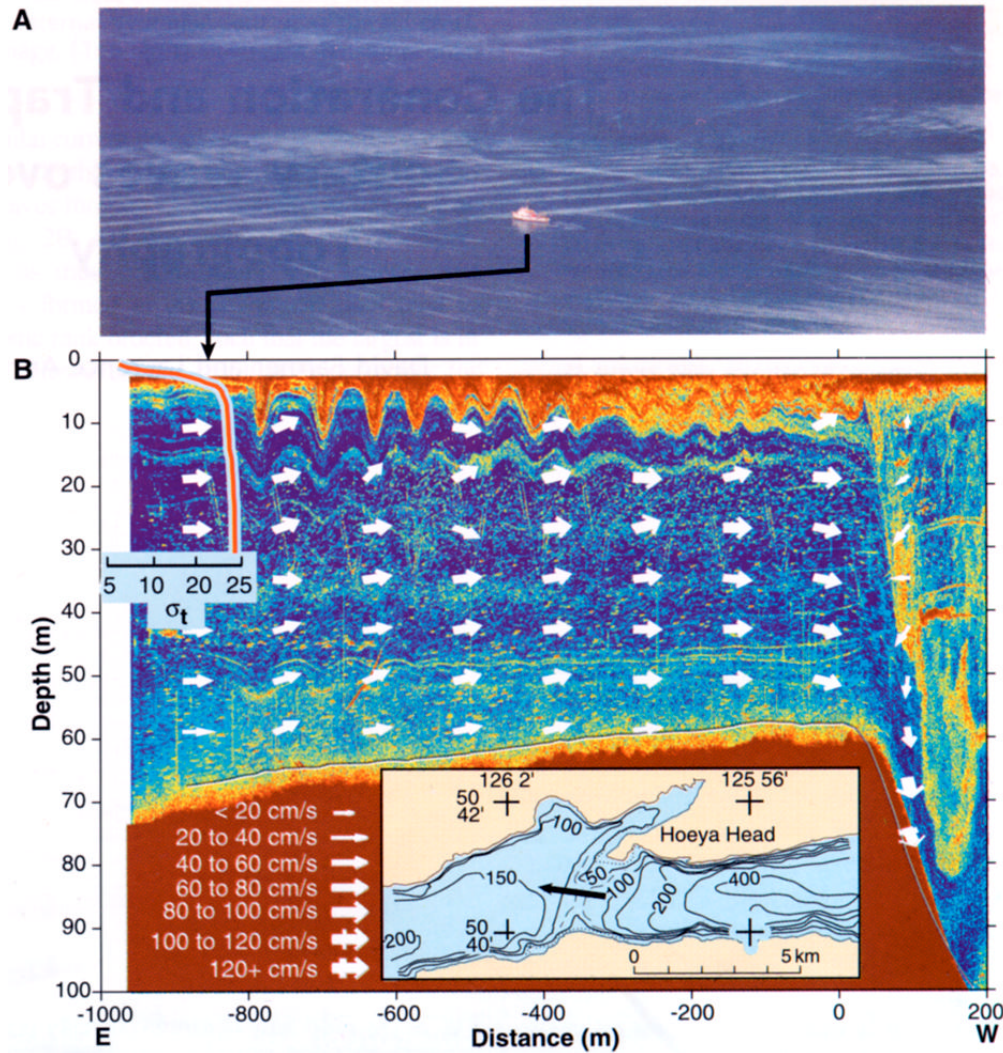**Oceanic Internal Waves and Solitons**

Fig. 11. (A) Photograph of Canadian ship *Vector* traversing packet of solitons in Knight Inlet, B.C. (B) Current vectors and acoustic profile during height of tidal flow. Ship direction is with current. Solitons appear to have been generated before release of downstream pycnocline depression. [*Farmer and Armi, 1999*.]

4.3 h, which time sees the onset of the undulatory bore. Approximately five oscillations have evolved by this point; other data to be presented ahead show that up to 30 solitons can develop to the east of Gibraltar over some 50 h. A several-hour depression of the thermocline with an amplitude of approximately one-half that of the lead soliton exists to the rear of the packet. Over the remainder of the tidal period, the system recovers to quasi-equilibrium or perhaps more accurately, to a quiescent state of internal displacements. The entire 12-1/2 h cycle constitutes the internal baroclinic tide in the region.

An Atlas of Oceanic Internal Solitary Waves (May 2002)   **Oceanic Internal Waves and Solitons**
by Global Ocean Associates
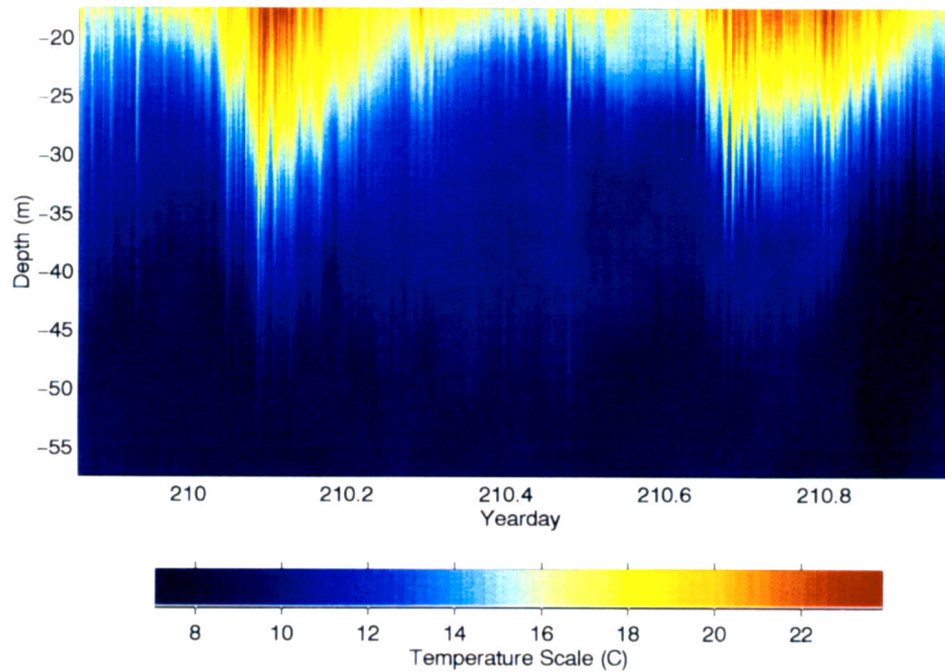Prepared for Office of Naval Research – Code 322 PO

Fig. 12. Soliton temperature excursions in summertime New York Bight during one day. Spikes are individual solitons; large groups are semi-daily tidal modulations. The slow recovery of temperature following the peak depression is typical of "solibore" behavior. Data courtesy of J. Lynch et al. (Apel et al., 1997).

Figure 10 illustrates a segment of an ERS-1 SAR image of the New York Bight just south of the Hudson Canyon, showing internal wave packets generated over the previous several tidal cycles. A nascent packet with one to two oscillations is seen forming near the center of the image; its position is very close to the shelf break, at a depth of 200 m. This demonstrates that the generation process takes place very near to the shelf break. At sills, it appears that generation occurs at approximately the same point in the geography.

An alternative mechanism to lee-wave generation is the direct production of rank-ordered solitons by shear-flow instability just up-current of the break/sill. Evidence exists from Knight Inlet, Canada, that near the maximum of tidal current, the velocity shear is great enough to excite solitons directly [Fig. 11; *Farmer and Armi, 1999*]. Because of nonlinearity, their propagation speed exceeds the instantaneous fluid speed, and they move against the current even during maximum flow. With the reversal of the tide, they accelerate and move with speeds that are the order of the summed phase and current velocities. It is thought that when the bartotopic tide slackens, the pycnocline depression, trying to maintain its former velocity relative to the water, may also slip up onto the shelf (or over the sill) and propagate as a more-or-less freely radiating wave [*Haury et al., 1979*]. A more detailed examination leads one to the conclusion that the soliton packets are actually the leading edge of an oscillating undulatory bore and that behind them, there is a longer-term depression of the equilibrium pycnocline lasting for much of the semidiurnal tidal period - a phenomenon termed a solibore by Henyey and Hoering [*1997*].

16

An Atlas of Oceanic Internal Solitary Waves (May 2002)   **Oceanic Internal Waves and Solitons**
by Global Ocean Associates
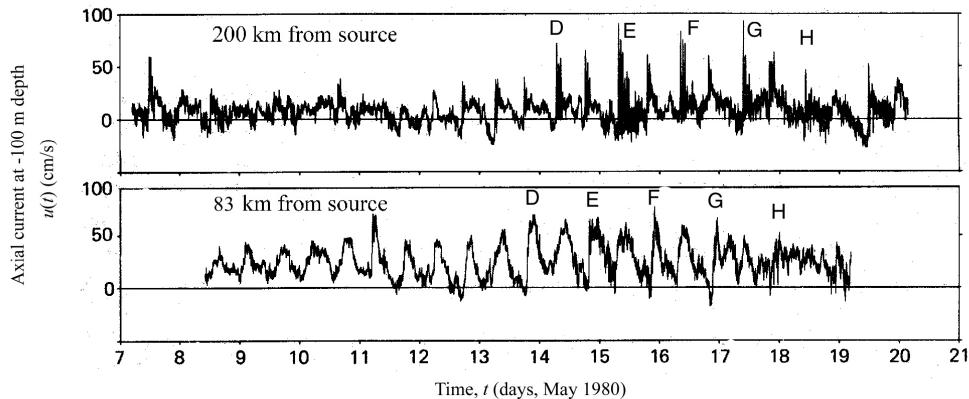Prepared for Office of Naval Research – Code 322 PO

Fig.13. Horizontal currents in direction of soliton phase propagation at 100 m depth in the Sulu Sea, P.I. spanning 10+ days. Locations at 83 km and 200 km from sill at Pearl Bank. Semidiurnal, diurnal, and fortnightly modulations are observed. Amplitudes exceed 100 m peak-to-trough for fully developed solitons. [*Apel et al, 1985*]

4.3 Propagation Phase

These kinds of processes may be repeated on each cycle of the semidiurnal tide, thereby producing effects like the several packets seen in Fig. 5. As time goes on, there are more and more oscillations added to the packet and it lengthens out. The distance between the packets is the wavelength of the internal tide and the velocity implied by that distance and the tidal period is the nonlinear velocity of the leading soliton, termed V_{max} in the theory. In-situ temperature data from moored thermistors in the New York Bight (Fig. 12) show two such cycles and illustrate the temporal behavior over more than a full diurnal period [*Apel et al., 1997*]. The long thermocline depression is apparent in this figure as well.

Over still longer times, the effects of the fortnightly cycle come into play. This is most clear in Fig. 13, which shows data from the Sulu Sea [*Apel and Holbrook, 1983; Apel et al., 1985; Liu et al., 1985*]. Here currents measured over approximately a ten-day period show semidiurnal/diurnal/fortnightly modulations, with the solitons present at spring tide and absent at neap tide. Semi-diurnal/diurnal asymmetries in soliton amplitudes and numbers are also visible, these arising from the mixed nature of the generating tides in the region. Such behavior strongly implicates the tides as forcing functions. Osborne and Burch [*1980*] have made similar observations in the Andaman Sea, west of the Malay Peninsula.

4.4 Dissipation Phase

It is in dissipation phase that the shelf- and sill-generated solitons differ the most. In the space beyond a sill, the soliton packets radiate and spread out, adding one new oscillation per buoyancy cycle and moving more or less free of bottom effects. There is some along-crest flow that causes the observed increases in crest lengths, probably at the expense of the potential energy stored in the trailing pycnocline displacements. There are also volume dissipations that appear to be more or less described by an eddy viscosity [*Liu et al., 1985; Liu, 1988*]. Measurements from the Sulu Sea imply lifetimes for the packets in excess of two days in deep water. Similar numbers are obtained from Gibraltar [*Wesson and Gregg, 1988; Apel, 2000*] and are consistent with open ocean observations made northeast of New Britain [*Pinkel et al., 1997*].

17

An Atlas of Oceanic Internal Solitary Waves (May 2002)   **Oceanic Internal Waves and Solitons**
by Global Ocean Associates
Prepared for Office of Naval Research – Code 322 PO

On the shelf, however, the waves suffer increasingly strong bottom interactions as the water shoals. Refraction due to both the shoaling depths and the (usually) decreasing pycnocline depth strongly orients the packet crests along isobaths, retards their speed of advance, and erodes their amplitudes. Development of a benthic boundary layer also occurs and leads to resuspension of bottom sediments and nutrients, often fertilizing the water column thereby [*Sandstrom and Elliott, 1984*]. Scattering from depth inhomogeneities contributes to additional attenuation. There is some evidence of the onset of shear-flow instability and roll vortices in very shallow water, of order 30 to 35 m in the New York Bight [*Orr, personal communication, 1995*]. In this regime, the soliton signatures have usually disappeared from images; in-situ observations suggest there are also suspended sediments and reduced optical transparency in the vicinity.

5. Theoretical Models

It is useful to first discuss the relatively simple first-order "quadratic" nonlinear soliton model, which was advanced by Korteweg and De Vries in 1897 to account for Lord Russell's observations. Since this original work, many additional solitary wave equations have been derived and new solutions found; one of special interest is the so-called "cubic" KDV equation. While there are undoubtedly physical applications for the newer theories, in the case of oceanic internal solitons, the so-called KDV or modified/combined KDV theories appear more or less satisfactory. While we will discuss these two equations, the more arcane theories will not be treated here, and we refer the reader instead to the review articles published in the last several years [*Ostrovsky and Stepanyants, 1989; Apel et al., 1998; Grimshaw et al., 1998*].

5.1 The Korteweg-de Vries Equation

When the development and propagation of a group of solitons is to be described, it is usual to resort to one of the "evolution" equations for KDV systems [*Liu et al., 1985*], which must be solved numerically, given initial data. Such an approach is reasonably successful if one includes both radial spreading from the source region and eddy dissipation. However, an analytical model giving some of the same physics is still desirable. We first discuss the model in terms of a two-layer system for simplicity, but later, in its application to actual situations, we use continuously varying vertical profiles of density and current.

In terms of separable solutions in x and z (neglecting the slow variations in the along-crest y-coordinate), solitons can be described by a product of (a) solutions to the weakly nonlinear Korteweg-de Vries equation for the traveling wave amplitude, $A(x, t)$, and (b) the eigenfunctions of the Taylor-Goldstein equation for the vertical structure function, $W_{k,n}(z)$. Here k is the horizontal component of wave vector and n is a vertical mode number. This structure function is discussed below, with the separability issue taken as given. Because the solutions involve both nonlinear and linear oscillations, the usual KDV limit of infinite wavelength, $k \rightarrow 0$, is not taken; the oscillatory solutions have finite wave numbers. This is different from the $\text{sech}^2(x)$ solution, for which $k \equiv 0$, and is numerically important as well.

The form of the total solution for the amplitude of vertical excursions of the pycnocline, $h(x,z,t)$, is taken as

$$h(x, z, t) = \sum_{n=1}^{n_{max}} h_{0n} W_{k,n}(z) A_n(x, t) \tag{1}$$

An Atlas of Oceanic Internal Solitary Waves (May 2002)   **Oceanic Internal Waves and Solitons**
by Global Ocean Associates
Prepared for Office of Naval Research – Code 322 PO

where h_{0n} is the amplitude for internal mode n and the sum is over the vertical modes present.

The Korteweg-De Vries equation for mildly nonlinear waves in shallow water is applicable to stratified fluids if (1) the ratio of the amplitude h to the upper layer depth h_1 is such that $h/h_1 \ll 1$ and (2), the wavelength is long compared with the upper layer depth: $[h_1/\Delta]^2 \ll 1$, where h_1 is the upper depth of the two-layer model and Δ the horizontal scale factor for soliton width. Of the two restrictions, the first is the more difficult to maintain in nature and typically this quantity is only slightly less than unity. In such a case, higher-order theory is called for. A review of past laboratory results for nonlinear waves [*Keulegan and Carpenter, 1961; Koop and Butler, 1981; Segur and Hammock, 1982; Kao et al., 1985*] suggests that the next-higher-order solution, while matching the waveform data somewhat better, makes only small changes in speed, etc., so that the dominant behavior is captured by the KDV theory. The treatment of the cubic KDV equation is deferred to the next section.

The quadratic one-dimensional Korteweg-de Vries equation can be written as

$$\frac{\partial A}{\partial t} + c_0 \left[\frac{\partial A}{\partial x} + aA\frac{\partial A}{\partial x} + g\frac{\partial^3 A}{\partial x^3} \right] = 0 \qquad (2)$$

where $A(x, t)$ gives the (normalized) vertical displacement of an isopycnal surface from its equilibrium level, and a, g, and c_0 are so-called environmental coefficients describing nonlinearity, dispersion, and long-wavelength phase speed, respectively. Note that the long wave speed c_0 has been factored out of the usual definitions of a and g, which allows their convenient interpretation in terms of characteristic lengths. It is also worth noting that the dispersion term involving $g A_{xxx}$ is itself a long-wave approximation, valid only when the actual wave number k is small compared with $1/(g^{1/2})$.

5.1.1   The Structure Function

Second-order differential equations govern the vertical structure function $W_n(z)$. In the case of fully nonlinear solitons moving with no background current, the limit $k \to 0$, is usually taken, and the equation for the (linear) vertical structure function is simply

$$\frac{d^2 W_n(z)}{dz^2} + \frac{N^2(z)}{c_0^2} W_n(z) = 0 \qquad (3)$$

where the Brunt-Väisälä or buoyancy frequency $N(z)$ is related to the density gradient via

$$N^2(z) = -\frac{g}{r}\frac{dr}{dz} \qquad (4)$$

However, this limit is not appropriate for the finite-k waves of the cnoidal/dnoidal type oscillatory solutions, but instead, the full Taylor-Goldstein equation for linear internal waves must be used. At the same time we generalize to allow for a streaming velocity (i.e. current) $U_0(z)$.

An Atlas of Oceanic Internal Solitary Waves (May 2002)   **Oceanic Internal Waves and Solitons**
by Global Ocean Associates
Prepared for Office of Naval Research – Code 322 PO

$$\frac{d^2 W_n(z)}{dz^2} + k^2 \left[\frac{N^2(z)}{[w_n - \mathbf{k} \cdot \mathbf{U_0}(z)]^2} + \frac{d^2 U_0 / dz^2}{k[w_n - \mathbf{k} \cdot \mathbf{U_0}(z)]^2} - 1 \right] W_n(z) = 0 \qquad (5)$$

The modified Taylor-Goldstein equation for the eigenfunction $W_{k,n}(z)$ is then where vertical variations in the buoyancy frequency, $N(z)$ and horizontal mean current velocity $\mathbf{U_0}(z)$ are allowed The wave frequency eigenvalue is ω_n for mode n. By allowing k to vary, the dispersion relation for the waves, $\omega_n = \omega(k)$ may be mapped out. Alternately the equation can be solved for eigenvalues of the phase speed, $c_n = c_n(k) = \omega_n / k$, where $c_n \to c_{0n}$ as $k \to 0$. (It should be noted that higher-order KDV approximations might require that the vertical eigenvalues $W_k(z)$ should depend on x as well. We will not tread that path here.) With the specification of upper and lower boundary conditions, this becomes a second-order Sturm-Liouville system. We impose rigid-lid boundary conditions at the surface, $z = 0$, and at the bottom, $z = -H$; in this case, $W_{k,n}(z)$ is then quantized into an integral number, n, of vertical "half-wavelengths."

Equation (5) is an extraordinarily rich and complicated one, with first and second-order poles located at $\omega_n = \mathbf{k} \cdot \mathbf{U_0}(z_{crit})$, indicating the possibility of critical levels or resonances in the fluid at $z = z_{crit}$. The term involving $U''_0(z)$ (the vorticity gradient) and its denominator change sign (and the equation thereby changes its properties) through the water column with daunting complexity. Additionally, shear-flow instabilities may occur if the Richardson number drops below 0.25 somewhere in the water column. Here the gradient Richardson number is

$$R_i \equiv \frac{N^2(z)}{[dU_0(z)/dz]^2} = \frac{N^2}{4\mathbf{v}^2} \qquad (6)$$

where $\mathbf{v} = \frac{1}{2}\nabla \times \mathbf{U}_0$ is the angular rotational velocity of a fluid with surviving vorticity component $\zeta_y = dU_0/dz$. Lindzen and associates have studied unstable shear flow effects in such fluids and have presented a rather clear picture of the requirements for instabilities to exist [*Orr, 1907; Lindzen, 1988*]. Lindzen demonstrates that, contrary to the view of Booker and Bretherton [1967], it is growth, rather than attenuation, that is possible near critical levels, depending on geometric and dynamic quantities. As a consequence, it should be noted that for short-wavelength waves, the phase speeds at which instabilities may develop are quite low, and even a modest background shear velocity can result in singular levels in the fluid, most usually located near the surface where wind-driven currents are the most intense [*Apel, 1999*].

There is experimental support for the use of the finite-k relationship, Eq.(5), in that KDV environmental parameters derived from those eigenfunctions yield improved propagation characteristics over the case for k =0. There is also experimental evidence that small solitons can be unstable against shear flow and develop into large, finite-amplitude waves rather than into roll vortices, as is the case with linear internal waves. Both Orr and Farmer and Armi privately report observations of shear-flow-induced vortex patterns in solitons, apparently without the concomitant destruction of the packet.

The TG equation can be modified to include effects of the Earth's rotation, which is important because at mid-latitudes, internal tidal periods are close to the Coriolis period. The resultant equation is more complicated and the solutions are altered, but mainly at very low

20

An Atlas of Oceanic Internal Solitary Waves (May 2002)   **Oceanic Internal Waves and Solitons**
by Global Ocean Associates
Prepared for Office of Naval Research – Code 322 PO

frequencies. There the linear case shows inertial oscillations propagating mainly in the vertical, and one would expect the nonlinear case to be somewhat similar. For an individual wave packet having periods of order 30 min, the effects are small. For several packets, the issue becomes more important. The rotational KDV equation is modified as well, with the differential order being raised by one and by the inclusion of a term given by $(f^2 \mathbf{h})/2c$, where f is the Coriolis parameter [*Ostrovsky, 1978; Ostrovsky and Stepanyants, 1989*]. Clearly, the present model is inadequate to handle rotation. Work on this is reserved for the future.

5.1.2 Environmental Coefficients

The basic environmental parameters describing the medium are the long-wave linear speed c_0, the dispersion factor $\gamma^{1/2}$ characterizing the scale over which a quadratic approximation for phase speed holds, and the quantity $\mathbf{a}^{-1}$ setting the maximum scale of the finite-amplitude nonlinearity. The phase speed c is the eigenvalue for the Sturm-Liouville problem above, and for long waves is approximated by the quadratic relationship

$$c(k) \cong c_0 (1 - \boldsymbol{g} k^2) \qquad (7)$$

This clarifies the meaning of c_0 as the eigenvalue at k =0, and γ as the coefficient in a quadratic expansion of *c(k)*. This expansion also illustrates the limitations of the shallow-water theory and the dispersion operator, γA_{xxx}. Integral dispersion operators covering a wider range of depths have been advanced by several authors [*Benjamin, 1966; Joseph, 1977; Kubota et al., 1978*].

The coefficients $\boldsymbol{a}$ and $\boldsymbol{g}$ can be evaluated from the integral relations given by Eqs. (9) to (11) below. However, their two-layer equivalents are listed first in order to provide an understanding of the factors controlling them, which are the upper layer thickness h_1, the lower layer thickness $h_2 = H - h_1$, and the density contrast,. $\Delta \boldsymbol{r} / \boldsymbol{r}$ across the layers. F or the two-layer fluid the environmental parameters are very simply

$$c_0 \cong \left(g \, \frac{\Delta \boldsymbol{r}}{\boldsymbol{r}} \, \frac{h_1 h_2}{h_1 + h_2} \right)^{\frac{1}{2}}, \qquad \boldsymbol{g} = \tfrac{1}{6} h_1 h_2, \qquad \text{and} \qquad \boldsymbol{a} = \tfrac{3}{2} \frac{(h_1 - h_2)}{h_1 h_2} \qquad (8)$$

Note that if $h_1 < h_2$, then $\boldsymbol{a} < 0$. Thus a thin upper layer results in downgoing displacements, for which $\boldsymbol{h} < 0$. This is the usual case in the ocean. When $h_1 = h_2$, the nonlinear coefficient vanishes and a higher-order KDV equation must be used. When the lower layer shoals to the point that $h_1 > h_2$, the sign of the displacement reverses and the solitons become upgoing. There are indications from remote sensing that such occurs in shallow water [*Liu et al., 1998*], although this also usually happens close to the point where strong bottom interactions take place.

In the case of a continuously stratified fluid, more complicated integral expressions must be substituted for these formulas. There are several versions of the integrals in the literature [*Benny, 1966; Lee and Beardsley, 1974; Maslow and Redekopp, 1980; Grimshaw, 1981; Suvorov, 1981; Liu and Benny, 1981; Rocklift, 1984*], differing significantly among themselves both theoretically and numerically, especially when shear flow is included. These have been informally reviewed by G. Watson [private communication, 1991]. For reasons of seeming mathematical rigor, the author (JRA) has chosen the formulation of Liu and Benny [*1981*].

An Atlas of Oceanic Internal Solitary Waves (May 2002)   **Oceanic Internal Waves and Solitons**
by Global Ocean Associates
Prepared for Office of Naval Research – Code 322 PO

Nonlinear Coefficient

$$a = \frac{3}{2Q} \int_H^0 \frac{c_0}{(c_0 - U_0)} \left(\frac{dW_n(z)}{dz} + \frac{dU_0/dz}{c_0 - U_0} W_n(z) \right)^3 dz \qquad (9)$$

Dispersion Coefficient

$$g = \frac{1}{2Q} \int_H^0 W_k^2(z) dz \qquad (10)$$

Normalizing Coefficient

$$Q = \int_{h_c}^0 \frac{c_0}{(c_0 - U_0)} \left(\frac{dW_n(z)}{dz} + \frac{dU_0/dz}{c_0 - U_0} W_n(z) \right)^2 dz \qquad (11)$$

In the last formula, h_c is the depth of a matching-inner-and-outer-expansion of the eigenfunction, and is typically several times the depth of the maximum value of $W_k(z)$. All of these depend on the suppressed modal index as well. In general, numerical solutions for $W_{k,n}(z)$ using continuously varying density and current profiles are required, since analytic solutions are available only for layered models or highly unrealistic analytical ones.

Because of the considerable differences found between the forms published in the literature, the numerical values of these coefficients must not be viewed as rigorously obtained. Additionally, under conditions wherein density and velocity profiles vary rapidly in the horizontal, or change under the influence of the solitons themselves, it is not always clear what the effective value of a, especially, should be.

It is important to note that because of the cubic factor in Eq. (9), a is very sensitive to the form of the structure function and its derivative, e.g., to the differences in the layer thickness, For example, if an upper layer isopycnal is displaced downward by a negative-going soliton or by the trailing thermocline depression, and at the same time a measurement is made of the density profile, an overestimate of the upper layer thickness will be obtained that is equal to the unperturbed layer depth plus the instantaneous soliton amplitude. If now a sequence of density profiles containing mainly down-going solitons is averaged over time, the result will be an overestimate of the average upper thickness as well as an underestimate of the lower thickness, resulting in a possibly bad value or even an incorrect sign for a. From numerical evaluation, it has been found that the multiplicative parameter ah_0 sensitively determines the number of solitons in a packet, and that a more nearly correct estimate of á (and hence the total number of solitons generated) may be derived by assuming that the proper layer thickness are those obtained from a pycnocline depth that is disturbed by the wave in the amount $2h_0$, rather than the undisturbed depth.

Figures 14(a) through (f) show how solutions for the structure function proceed. Figures 14(a) to (c) illustrate an undisturbed density profile (*Cournelle, personal communication, 1999*); a B-V profile, and two mean velocity profiles for the central Strait of Gibraltar during the spring (Watson and Robertson 1991). Figures 14(d) to (f) show the eigenfunctions for the first mode, the linear phase speed, and the dispersion relations for this mode as well. The long-wave eigenvalue c_0 is the intercept of the phase speed curves at the k-origin, and this is a fundamental quantity for the KDV solutions. The presence of velocity shear only slightly changes the Mode 1

An Atlas of Oceanic Internal Solitary Waves (May 2002)
by Global Ocean Associates
Prepared for Office of Naval Research – Code 322 PO

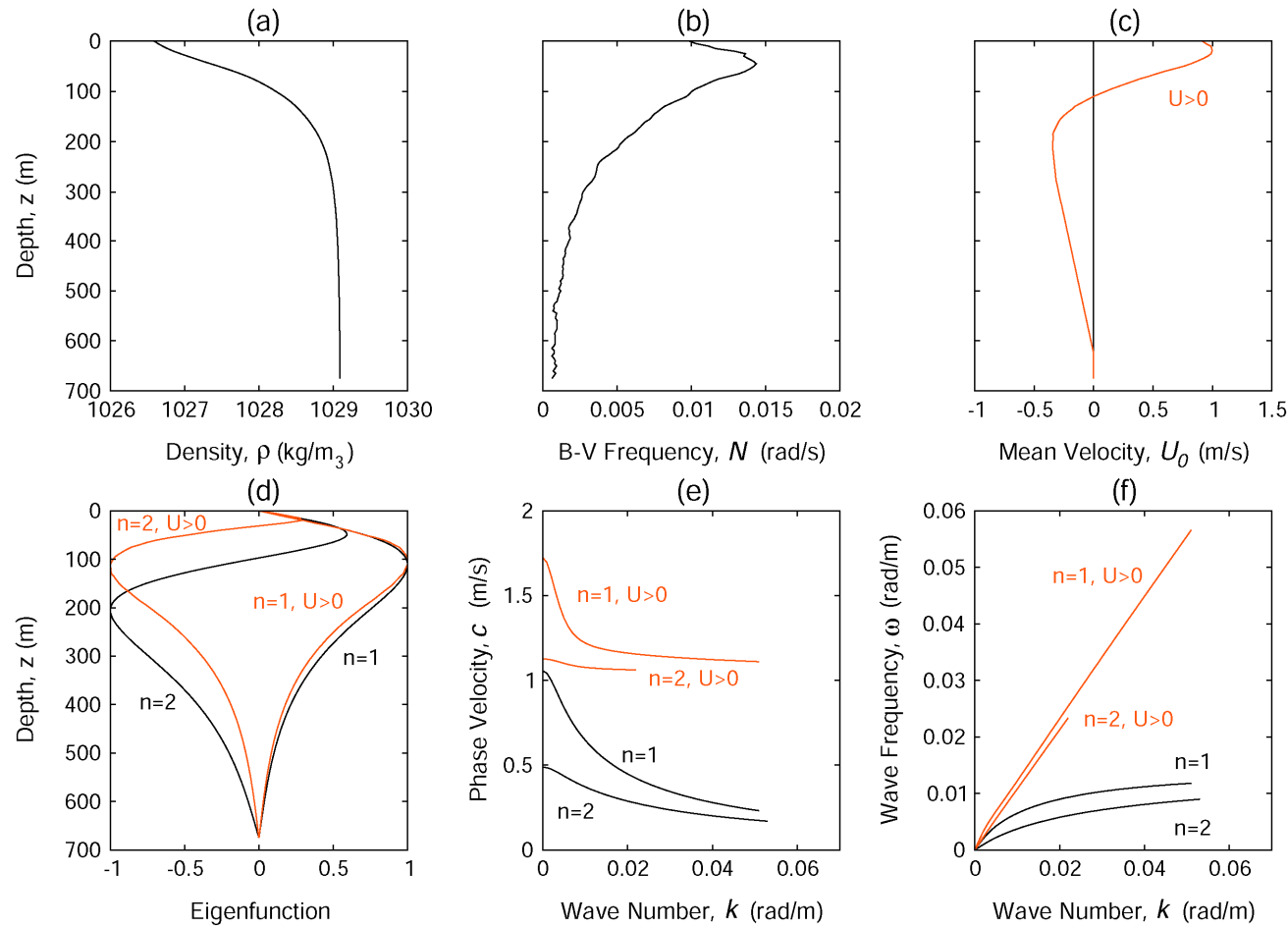Oceanic Internal Waves and Solitons

Figure 14. Solution procedure for the structure function. a) Typical undisturbed Density Profile for Gibraltar b) derived Brunt-Väisälä frequency $N(z)$ c) current flow profile d) Normalized vertical eigenfunctions (mode 1 & 2) for $2\pi/k_0 = 900$ m, H = 675 m for density and velocity profiles shown e) Phase Velocity f) Dispersion relations. The red curves show the results with current (U > 0).

An Atlas of Oceanic Internal Solitary Waves (May 2002)   **Oceanic Internal Waves and Solitons**
by Global Ocean Associates
Prepared for Office of Naval Research – Code 322 PO

eigenfunction, but substantially modifies Mode 2 (Fig.14(d)). The background velocity also bodily advects the wave packet at a speed that is vertically weighted in some fashion by the structure function (Fig. 14(e)). This effect adds to the intrinsic phase speed and moves the centroid of the packet forward at the calculated value c_0 ƿ 1.7 m/s. In the absence of a mean current, c_0 is close to 1 m/s. Thus, the observed frequency is Doppler-shifted to high values.

5.2 The KDV Solution

5.2.1 Hyperbolic Secant Profile

If the shallow water approximation holds, then the prototypical analytical solution for a single soliton pulse is

$$A(x,t) = 2\boldsymbol{h}_0 \sec h^2 \left(\frac{x - Vt}{\Delta} \right) \tag{12}$$

where V is the nonlinear phase speed and Δ is a measure of the width of the squared hyperbolic secant pulse and is itself a function of $\boldsymbol{h}$, $\boldsymbol{a}$ and $\boldsymbol{g}$. The amplitude is written as $2\boldsymbol{h}_0$ to facilitate comparison with the oscillating solutions ahead. For single solitons, the invariant shape of the KDV solution and its dependencies on the amplitude and the environmental parameters have been surprisingly well-verified both in the ocean [*Apel et al., 1985; Liu et al., 1985; Ostrovsky and Stepanyants, 1989; Apel et al., 1998*] and in hydrodynamic tanks [*Keulegan and Carpenter, 1961; Koop and Butler, 1981; Segur and Hammock, 1982; Kao et al., 1985*]. Figure 15 shows the shape of the classic soliton solution in a stratified fluid; the figure serves to define the parameters of the single-pulse model.

For this model, the characteristic width Δ is related to the amplitude and environmental coefficients via

$$\Delta = \sqrt{\frac{6\boldsymbol{g}}{\boldsymbol{a}\boldsymbol{h}_0}} \tag{13}$$

For moderate–to-large-amplitude waves, this relationship is in general obeyed, but is sometimes found to be only very approximately correct [*Apel et al*., 1985; *Kropfli et. al* 1999], presumably because of higher-order non-linear effects (see ahead). Nevertheless, it relates the characteristic scale Δ, which is often directly observable in images or from in-situ data, to the vertical excursion, $\boldsymbol{h}_0$, which is not. One requires values of $\boldsymbol{a}$ and $\boldsymbol{g}$ in order to obtain an amplitude measure, but these can often be estimated for the geographical location and season from historical data.

The nonlinear speed *V* can be similarly estimated via the relationship derived from KDV theory,

$$V = c_0 \left(1 + \frac{2}{3} \boldsymbol{a}\boldsymbol{h}_0 \right) \tag{14}$$

Often two or more tidally generated packets are visible in a wide-swath image, and from the knowledge of tidal periods, *T* ƿ 12½ and 25 h, estimates can be made of the maximum nonlinear velocity Vmax from the interpacket separation: *D* ƿ V_{max}T. These velocities range

24

An Atlas of Oceanic Internal Solitary Waves (May 2002)   **Oceanic Internal Waves and Solitons**
by Global Ocean Associates
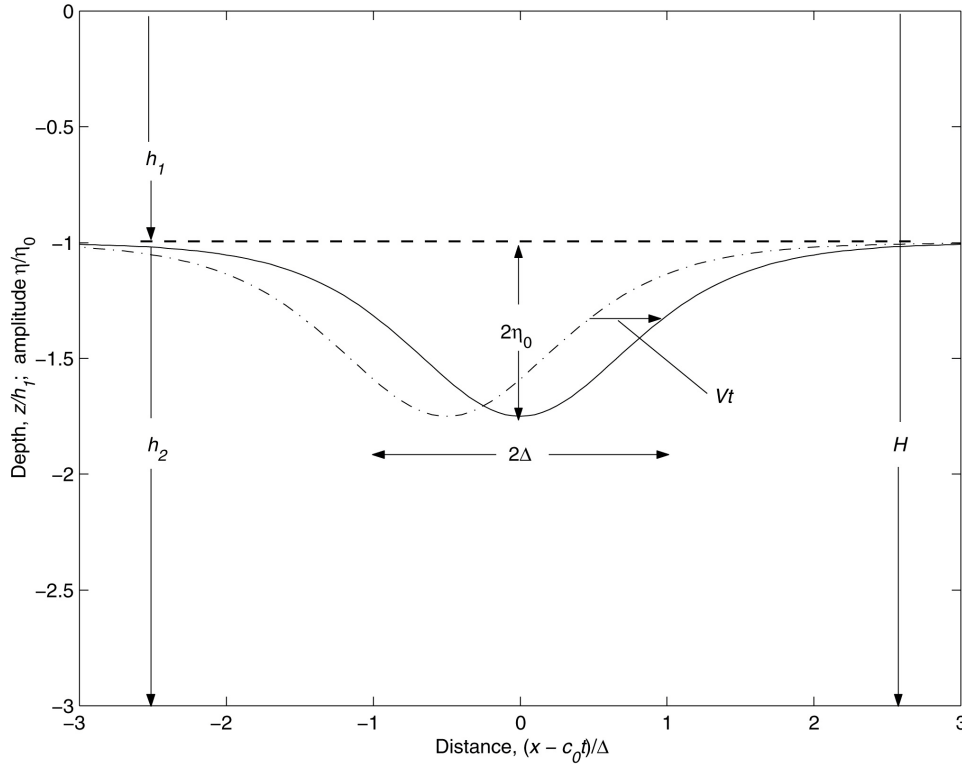Prepared for Office of Naval Research – Code 322 PO

Figure 15. Classic $\text{sech}^2(x)$ profile for KDV soliton at two different times, viewed in coordinate system moving with longwave linear speed, c_0.

from approximately 0.5 to 2.0 m/s under usual conditions, for which inter-packet separations are of order 25 to 100 km.

The authors believe that the KDV theory captures most of the variance in the observations and that the higher-order refinements, while interesting and useful, do not negate the utility of the Korteweg-de Vries formulation.

5.2.2   The Cnoidal Profile

While the single-pulse KDV soliton is mathematically simple, one finds that in place of single pulses in the ocean there are almost always packets consisting of several oscillations of a quasi-periodic nature, with decreasing wavelengths, crest lengths, and amplitudes occurring from the front to the rear of the wave group; the data of Section 4 demonstrate this clearly. Now Korteweg and de Vries also published a nonlinear periodic solution in their 1898 paper, the so-called cnoidal wave involving the Jacobian elliptic function, $cn_s(x)$. This function has a free parameter, s, that establishes the degree of nonlinearity: $0 \le s^2 \le 1$. The KDV cnoidal solution is given by
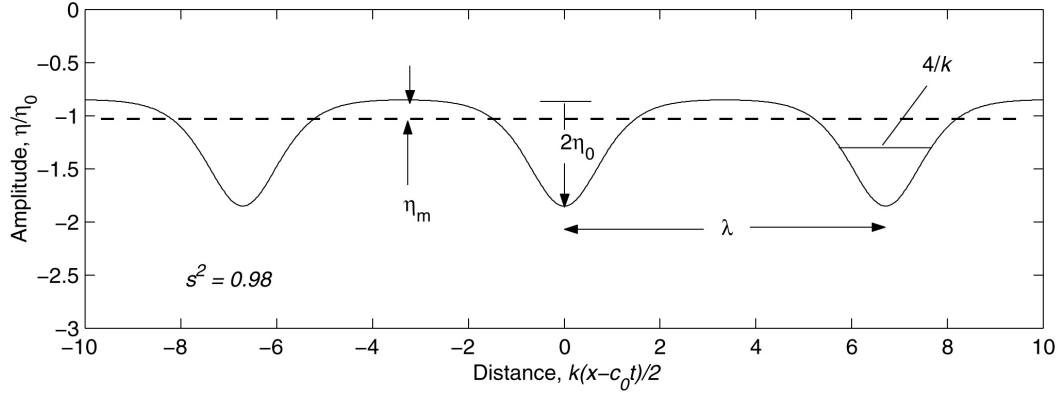
An Atlas of Oceanic Internal Solitary Waves (May 2002)   **Oceanic Internal Waves and Solitons**
by Global Ocean Associates
Prepared for Office of Naval Research – Code 322 PO

Figure 16: KDV periodic cnoidal solution showing three cycles of uniform solitons with nonlinear parameter $s^2 = 0.98$.

$$A(x,t) = \boldsymbol{h}_m + 2\boldsymbol{h}_0 cn_s^2 \left[\frac{1}{2} k_0 (x - Vt) \right] \tag{15}$$

Where η_m and η_0 are amplitude factors and k_0 is a wave number. Figure 16 shows the cnoidal waveforms for $s^2 = 0.98$ and defines several of the lengths. When $s \rightarrow 0$, $cn_s(x) \rightarrow \cos(k_0(x - Vt)/2)$ and the linear oscillatory solution is recovered. As $s \rightarrow 1$, $cn_s(x) \rightarrow \mathrm{sech}(x)$, and the individual oscillations have stretched infinitely far apart, leaving the single-pulse soliton. Thus $cn_s^2(x)$ is a generalization of the better-known $\mathrm{sech}^2(x)$ solution, but also reduces to the sinusoidal wave with small nonlinearity. The so-called "stretched wavelength," λ, the distance between successive minima or maxima, is given by

$$\boldsymbol{l}(s) = \frac{4K(s)}{k_0} \tag{16}$$

where $K(s)$ is the complete elliptic integral of the first kind. The important wave number k_0 is related to Δ for the single-pulse soliton (and in turn to $\boldsymbol{a}$, $\boldsymbol{g}$, and $\boldsymbol{h}_0$) and is given by

$$\frac{1}{2} k_0 = \sqrt{\frac{\boldsymbol{a}\boldsymbol{h}_0}{6\boldsymbol{g}}} \qquad \text{or} \qquad \boldsymbol{h}_0 = \frac{3\boldsymbol{g}k_0^2}{2\boldsymbol{a}} \tag{17}$$

The wave number k_0 plays a dual role in the cnoidal function. On one hand, it gives the characteristic width of each oscillation of the cnoid, which is related to the KDV soliton width as $k_0/2 = 1/\Delta$, a quantity that is constant throughout the wave packet. On the other hand, it is also the wave number of the linear $\cos(k_0x)$ solution at the rear of the packet. Thus, it is a scale factor that remains valid throughout the entire range of x, from fully nonlinear to fully linear, and will constitute a very important quantity in the analysis of observational wave packets ahead.

However, the cnoidal wave packet model has several ad-hoc assumptions associated with it, and additionally there is no clear way to allow it to develop into a propagating, evolving

An Atlas of Oceanic Internal Solitary Waves (May 2002)   **Oceanic Internal Waves and Solitons**
by Global Ocean Associates
Prepared for Office of Naval Research – Code 322 PO

model with the possible exception of the approach advanced by Osborne [*1995*]. Most importantly, it does not contain the pervasive characteristic of observed soliton packets mentioned above, e.g., a sharp onset and a long-term trailing-edge depression of the isopycnal surfaces behind the wave group. These deficiencies of the cnoidal model have resulted in the adoption of another solution to the KDV equation that I (JRA) term the "dnoidal" solution

5.2.3   The Dnoidal Profile

Gurevich and Pitaevskii (*1973 a, b, 1990*) have utilized a relatively unknown solution to the KDV equation to describe collisionless shock waves in plasma, a solution that is given in terms of another of the Jacobian elliptic functions, $dn_s(\xi)$. (The "collisionless" property is due to the fact that solitons, like collision-free particles, interact with each other with no net change in energy.) The dnoidal function is also an oscillatory quantity that approaches $\text{sech}(\xi)$ as the parameter $s^2 \rightarrow 1$, but in contradistinction to $cn_s(\xi)$, approaches unity as $s^2 \rightarrow 0$. Now there is a trigonometric relationship between $dn_s(\xi)$ and $cn_s(\xi)$, viz.:

$$dn_s^2(\boldsymbol{x}) - (1 - s^2) = s^2 cn_s^2(\boldsymbol{x}) \tag{18}$$

Then for constant s^2, the KDV cnoidal solution can readily be written in terms of the dnoidal function. However, in the solution by Gurevich et al. [*1973*], $dn_s^2(\boldsymbol{x})$ is used with an additional relationship that is produced by allowing a slow variation of s^2 within the wave packet, as well as by imposing theoretical limits on the range of the independent variable ξ. The resultant solution then takes on significantly different properties from $cn_s^2(\boldsymbol{x})$. It turns out that this form of the dnoidal function is particularly well adapted to model the response of a fluid to an initial sharp impulse that induces "ringing" along its leading edge. The $dn_s^2(\boldsymbol{x})$ model possesses the all-important properties of a rapid onset (the shock front), the development of additional oscillations, increases in packet lengths as space and time go on, and a long-term depression of the trailing end of the packet. As was discussed above, this trailing depression is an important property of naturally occurring internal soliton packets.

Apel [*2001*] contains a short derivation of the Gurevich and Pitaevskii (GP) solution. The basis for the derivation can be found in their papers in JETP, although in somewhat different form, and the reader is directed to these references for its justification. In a more recent paper, Gurevich and colleagues (*1990*) amplify on the properties of the solution.

Here we are interested in its application to the oceanic soliton case, and the Gurevich and Pitaevskii formulation, originally done for plasmas, has been modified to apply to the slow oscillations of an uncharged, stratified, streaming fluid such as the ocean. This primarily consists of redefining the KDV parameters to apply to that case, and generally follows the work of Benjamin [1962, 1966] and Benny [1966].

For initial conditions approximating an impulse exerted on the fluid at $(x, t) = 0$, the periodic $dn_s^2(\boldsymbol{x})$ soliton solution to the Korteweg-deVries equation is given by

$$A(x,t) = \boldsymbol{h}_0 \left\{ 2 dn_s^2 \left[\tfrac{1}{2} k_0 (x - Vt) \right] - (1 - s^2) \right\} + \boldsymbol{h}_m \tag{19}$$

An Atlas of Oceanic Internal Solitary Waves (May 2002)   **Oceanic Internal Waves and Solitons**
by Global Ocean Associates
Prepared for Office of Naval Research – Code 322 PO

Here h_0 is an amplitude factor (to be determined by external factors); k_0 is a wave number dependent on the KDV environmental parameters; V is the nonlinear phase speed; and h_m is a quantity to be determined by other considerations.

In their 1990 paper, Gurevich et al. claim that Eq. (19) is the general solution to the KDV equation, (2), and cite their 1973 papers as proof. The trigonometric relationship between dn and cn, Eq. (18), is such that this solution would have the same generality as Eq. (12); but as will be seen below, its behavior is clearly different when the initial conditions and the variations in s are imposed.

The important theoretical relationship between the KDV environmental parameters and the short-wavelength wave number k_0 now takes the form

$$\frac{1}{2} k_0 = \sqrt{\frac{ah_0}{6g}} \qquad \text{or} \qquad h_0 = \frac{3gk_0^2}{2a} \tag{20}$$

This allows one to estimate the displacement amplitude, knowing k_0, a, and g from field data, for example. (There is clearly a problem with Eq.(20) as $\alpha \rightarrow 0$. Then the cubic KDV must be invoked.) In addition, the nonlinear phase speed at the front of the packet, which is given by

$$V = c_0 \left(1 + \frac{1+s^2}{3} ah_0 \right) \rightarrow c_0 \left(1 + \frac{a(2h_0)}{3} \right) \equiv V_{kdv} \qquad \text{as } s^2 \rightarrow 1 \tag{21}$$

can then be estimated from these data as well. (The second expression above shows the dnoidal phase speed approaches the classic nonlinear speed for an isolated soliton with amplitude $2h_0$) These equations are exact theoretically but work with varying degrees of accuracy in practice, probably because of the non-inclusion of higher-order nonlinearities.

The nonlinear parameter s^2 remains unspecified at this point and must be established by other means. Where the KDV cnoidal solution simply assumed it is a constant related to the amplitude parameters. Gurevich and Pitaevskii [*1973a, b*] allowed it to vary slowly in order to construct a packet, so that $s = s[\tau(x)]$, as obtained from rate equations for the slower variations. In terms of a space-time ratio, τ, which is defined only over the packet extent, their solution for s^2 is given implicitly via

$$t \equiv \frac{x'}{h't'} \equiv \frac{x - c_0 t}{ah_0 c_0 t} = \tfrac{1}{3}(1 + s^2) - \tfrac{2}{3} \frac{s^2(1-s^2)K(s)}{E(s) - (1-s^2)K(s)} \tag{22}$$

Here $K(s)$ and $E(s)$ are complete elliptic integrals. (The usual notation for the argument of these integrals is $m = s^2$ and $K(m) = K(s^2)$. We retain the present notation for conformity to the GP references.) The transformation of variables used in arriving at this relationship has mapped the semi-infinite half space, $x - c_0 t \geq 0$ to a finite interval in τ defined by $-1 \leq \tau \leq 2/3$, for $0 \leq s^2 \leq 1$; this interval thereby establishes the packet length. Since τ is a space-time ratio, the packets can differ in their actual wavelengths, number of oscillations, etc. in physical space while remaining confined to this interval. Also, $\tau = 0$ defines that point in the packet traveling with the long-wavelength speed c_0, which is effectively the centroid of the wave group; from the range of
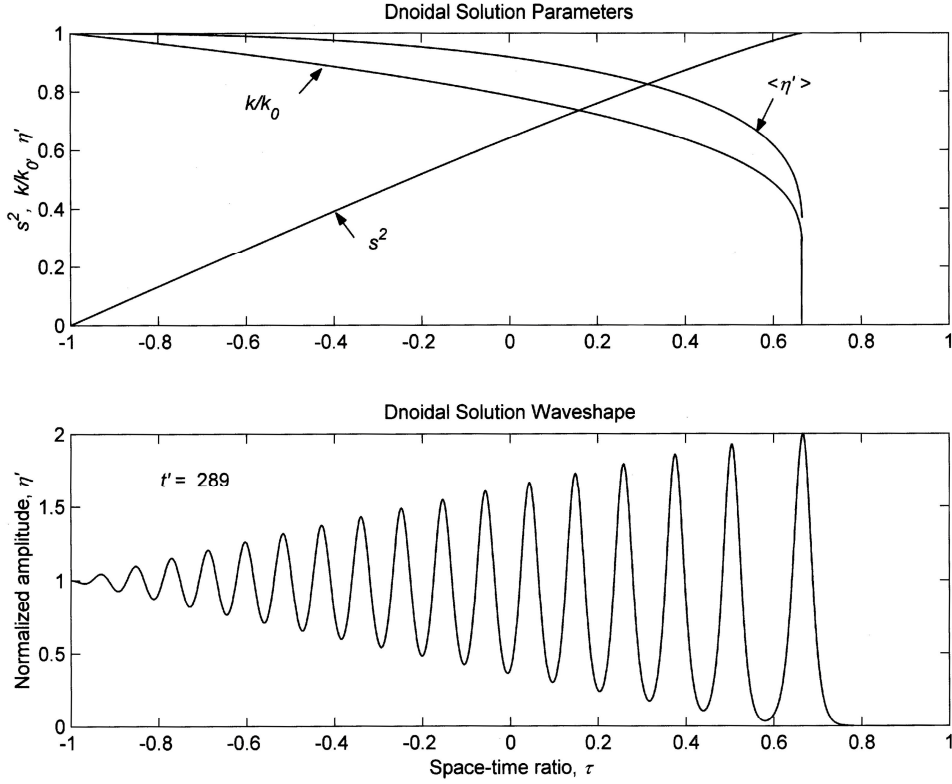
An Atlas of Oceanic Internal Solitary Waves (May 2002)   **Oceanic Internal Waves and Solitons**
by Global Ocean Associates
Prepared for Office of Naval Research – Code 322 PO

Figure 17 (Upper) Theoretical behavior of normalized parameters in dnoidal solution, vs. t, using Eq. (12) for s^2. Beyond $\tau = 2/3$, $s^2 \equiv 1$. (Lower) Normalized amplitude at $\tau' = 289$. Beyond $\tau = 2/3$, the classic $\text{sech}^2(\tau)$ solution extends wave into evanescent region.

τ, this is at a distance of 2/5ths of the packet length from the lead wave. In physical space it is at a distance $x = c_0 t$ from the origin. The coordinate origin is placed at the position of the impulse application - the shelf (or sill) break - and t =0 is taken as the time of reversal of the tidal flow at the break and the release of the downstream depression (or generation of the shear instability).

The direct solution for $s^2 = s^2(\tau)$ from the non-algebraic Eq. (12) is difficult; on the other hand, given s, the inverse solution $\tau = \tau(s^2)$ is simple [*Gurevich and Pitaevskii, 1973a, b*]. A graphical inversion as a function of τ is shown on Fig. 17, where it may be seen to have the range and domain stated. Also in Fig. 17 this figure are shown the variation in normalized wave number, k/k_0 and the amplitude averaged over a wavelength, $\langle h/h_0 \rangle$. These are given by

$$\frac{k}{k_0} = \frac{p}{2K(s)} \tag{23}$$

and

An Atlas of Oceanic Internal Solitary Waves (May 2002)   **Oceanic Internal Waves and Solitons**
by Global Ocean Associates
Prepared for Office of Naval Research – Code 322 PO

$$\left\langle \frac{\boldsymbol{h}}{\boldsymbol{h}_0} \right\rangle = \frac{2E(s)}{K(s)} + s^2 - 1 \qquad (24)$$

Both approach zero logarithmically at the front of the packet and unity at the tail. Thus it may be seen that at the front of the packet,

$$\tau \to 2/3, \qquad s^2 \to 1, \qquad k \to 0, \qquad V \to V_{kdv}$$

where V_{kdv} is the fully nonlinear velocity of the KDV solution, while at the rear of the packet,

$$\tau \to -1, \qquad s^2 \to 0, \qquad k \to k_0, \qquad V \to c_0$$

The packet centroid moves with the long-wave linear velocity c_0. This characteristic is useful in interpreting observational data containing multiple packets.

Figure 17 also illustrates the form of the $dn^2_{s(x)}(\boldsymbol{x})$ amplitude function of Eq. (19), using Eq.(22) and normalized variables. The function clearly shows waveforms that are non-cosinusoidal near the front but which approach linear cosinusoidal shapes at the rear. The diminution of amplitudes and wavelengths are apparent as well. It also demonstrates that the constant trailing amplitude of $\boldsymbol{h}_0$, or one-half the peak-to-trough amplitude of the leading wave, is due to the properties of the dnoidal function when taken together with the s^2 variation; it is here that the $dn_s(\xi)$ and $cn_s(\xi)$ solutions differ the most. The interpretation of the downward-displaced tails in Figs.7 and 9 can then made in such terms. Thus, this solution has many of the basic properties observed in internal solitons in the ocean.

As time advances, the number of oscillations increases, one per buoyancy period. Some soliton theories regard this number as being determined by the "strength" of the "potential well" embodied in the downward displacement of the pycnocline, with any left-over energy leading to a linear dispersive tail at the rear of the generation region (see *Dodd et al. 1982*, for example). The present theory gives an alternative viewpoint, suggesting that a continuous diminution of wave nonlinearity takes place from front to back. The distance between successive solitons, the so-called stretched wavelength λ, is, from Eq. (23),

$$\boldsymbol{l}(s) = \frac{4K(s)}{k_0} = \frac{2\boldsymbol{p}}{k} \geq \frac{2\boldsymbol{p}}{k_0} = \boldsymbol{l}_0 \qquad (25)$$

Here $\lambda_0 = 2\pi / k_0$ is the wavelength at the trailing end of the packet, and is an important quantity in interpreting field data in terms of the model. The period between successive passages of individual oscillations is

$$T = \frac{\boldsymbol{l}}{V} = \frac{4K(s)}{k_0 V} \qquad (26)$$

both of which decrease toward the rear of the packet.

An Atlas of Oceanic Internal Solitary Waves (May 2002) **Oceanic Internal Waves and Solitons**
by Global Ocean Associates
Prepared for Office of Naval Research – Code 322 PO

It should be noted that the dnoidal solution (19) is not accurate at extremely short times, during the very early response to the imposed shock. Now near the point $\tau = 2/3$, one has $s^2 \rightarrow 1$; the solution ahead of that distance may then be obtained by appending one-half of the waveform of *any* of the fully nonlinear KDV solutions (including solutions of the cubic KDV equation, for example). If the appended waveform is that of the $\text{sech}^2(\tau)$ profile, the results are as shown on Fig.17. It is thus seen that at $\tau = 2/3$, the nature of the solution changes from oscillatory to evanescent, much as does the wake of a ship at the Kelvin caustic, which is also a shock-like phenomenon.

5.2.4   The Dnoidal Model

The dnoidal *model* is an extension of the dnoidal *solution* that more closely simulates observed solitons and their associated nonlinear internal tides, with the expectation of improved fidelity, given the correct numerical choice of parameters [*Apel 2003*]. By including the vertical structure function $W_{k,n}(z)$ and a long-wavelength modulation function $I[(x-c_0t)/(c_0T_l)]$

that describes the depressed trailing edge of the internal tide on the continental shelf and its attenuation, the model may be written as

$$\boldsymbol{h}(x,z,t) = \sum W_k(z)\left\{2\boldsymbol{h}_0 dn_s^2\left[\tfrac{1}{2}k_0(x-Vt)\right] - \boldsymbol{h}_0(1-s^2)\right\} \times I\left[\frac{x-c_0t-\boldsymbol{c}}{c_0T_l}\right]\exp(-\boldsymbol{a}_{att}x) \quad (27)$$

where the sum is over those normal modes excited but where the modal index has been suppressed. The internal tide recovery function I is taken to be a hyperbolic tangent with a horizontal scale c_0T_l, of the form

$$I(x,t) = \frac{1}{2}\left\{1 + \tanh\left[\frac{x-c_0t-\boldsymbol{c}}{c_0T_l}\right]\right\} \quad (28)$$

This function is attached to the dnoidal solution at a distance χ from the centroid and moves toward increasing x at the long-wave linear phase speed c_0. The exponential attenuation function describes the effect of dissipative forces at work during the propagation of the packet (see Section 4.4). Numerical values from the Sulu Sea and Gibraltar imply a packet lifetime, $T = 1/(\boldsymbol{a}_{att}V)$ of roughly two days. Figure 18 shows the space and time evolution of a dnoidal wave packet and illustrates, in moving coordinates, the increase in number of solitons and their wavelengths, the lengthening of the packet, and the attenuation of the amplitudes that are part of Eq.(22).

The parameters χ and T_l are chosen to give agreement with observation, with c_0T_l giving a spatial scale to the hyperbolic tangent function, and χ establishing a horizontal displacement of the midpoint at I =1/2 from the packet centroid. The recovery function is attached to the centroid of the dnoidal wave packet at the position x = c_0t + χ and moves with the speed c_0. Parameter values for the scaling of I(x, t) are typically Tl þ 2 h and $\chi \approx$ 0-4 km. A simple attenuation function is used to diminish the amplitudes. Its form is exp [-a (x - x$_a$)] where x$_a$ =1 km, and a þ 2×10^{-2} km^{-1} , values that derive from experience in the Sulu Sea and elsewhere.

An Atlas of Oceanic Internal Solitary Waves (May 2002) **Oceanic Internal Waves and Solitons**
by Global Ocean Associates
Prepared for Office of Naval Research – Code 322 PO
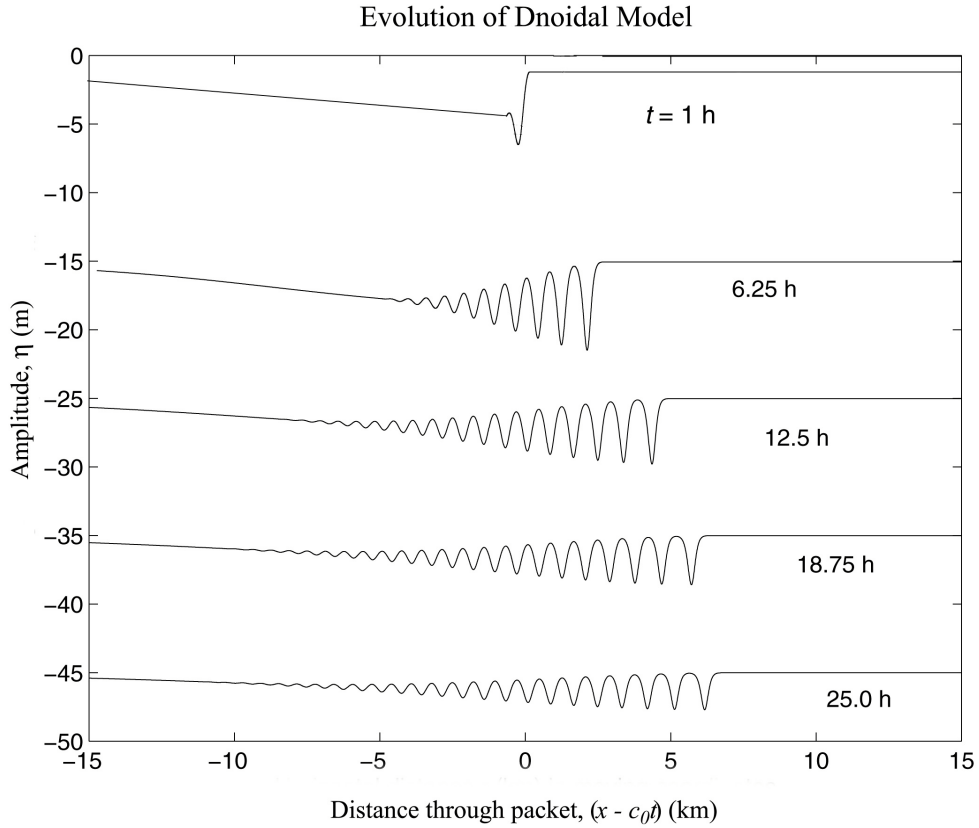
Evolution of Dnoidal Model

Figure 18. Dnoidal model evolution over one diurnal tidal period. Model modifies solution by includes the vertical structure function, attenuation, and recovery of the trailing edge to small values later in packet. One cycle is added each buoyancy period.

This relationship has been applied to data from the field program entitled "Shallow Water Acoustics in Random Media" (SWARM–discussed elsewhere in this book); to data from several other field programs; and to more casual observations of internal solitons via remote and in-situ sensing. In general, reasonable-to-good agreement is obtained between theory and observations.

5.3 Combined/Modified KDV Equations
When the wave amplitude exceeds the upper layer depth, a higher-order expansion is necessary. The combined KDV relationship then becomes

$$\frac{\partial A}{\partial t} + c_0 \left[\left(1 + \boldsymbol{a}A + \boldsymbol{a}_3 A^2 \right) \frac{\partial A}{\partial x} + \boldsymbol{g} \frac{\partial^3 A}{\partial x^3} \right] = 0 \tag{29}$$

An Atlas of Oceanic Internal Solitary Waves (May 2002)   **Oceanic Internal Waves and Solitons**
by Global Ocean Associates
Prepared for Office of Naval Research – Code 322 PO
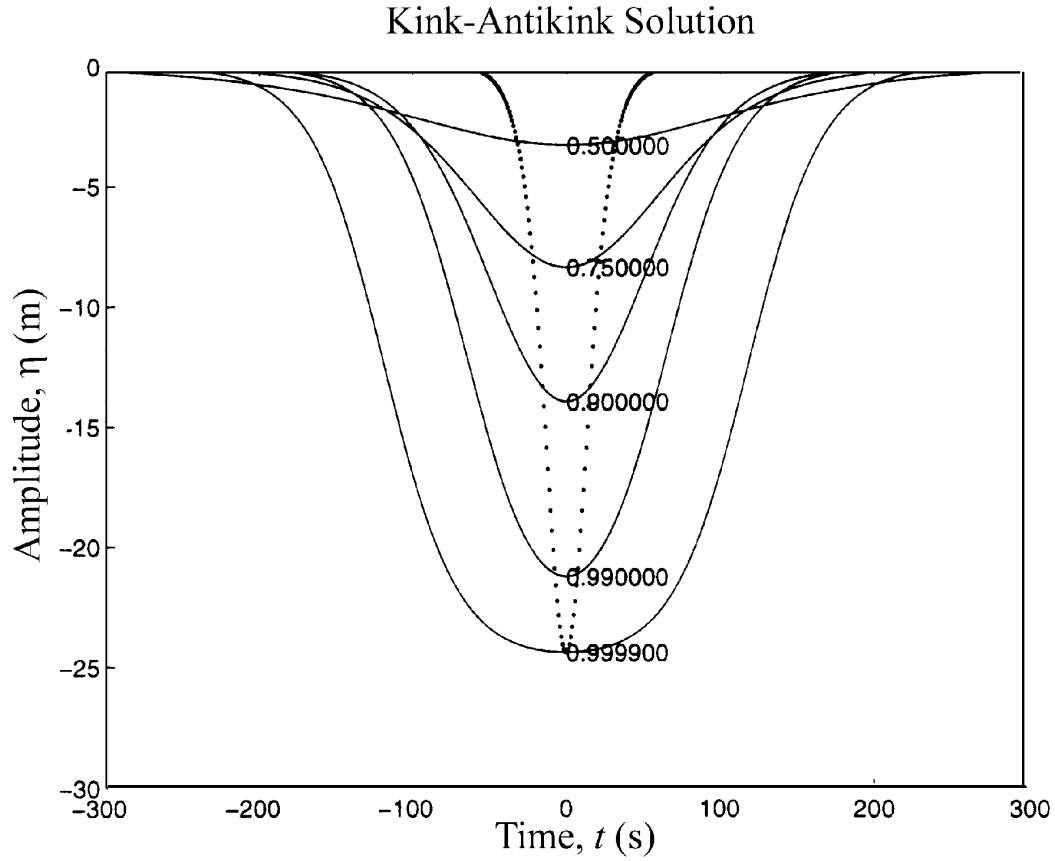
Kink-Antikink Solution

Figure 19. "Kink-antikink" solution for solitons with cubic nonlinearity and varying degrees of the nonlinear parameter, **n**. The dotted curve is the classic KDV soliton. Figure courtesy of T. P. Stanton and L. Ostrovsky (1999).

where the coefficient of the cubic term is a_3 [*Lee and Beardsley, 1974; Ostrovsky and Stepanyants, 1989*]. While the sign of a depends on the layer depths (cf. Eq. (3)), it turns out that a_3 is always negative. For a two-layer fluid a_3 is

$$a_3 = \frac{3}{h_1^2 h_2^2}\left[\tfrac{7}{8}(h_2 - h_1)^2 - \left(\frac{h_2^3 + h_1^3}{h_1 + h_2}\right)\right] \qquad (30)$$

The environmental parameters c_0, α and γ are the same as those in the weakly nonlinear KDV equation. In this case, the CombKDV equation is fully integrable, with the displacement being in the form of a kink-antikink pair of solutions involving hyperbolic tangents:

33

An Atlas of Oceanic Internal Solitary Waves (May 2002) **Oceanic Internal Waves and Solitons**
by Global Ocean Associates
Prepared for Office of Naval Research – Code 322 PO

$$A(x,t) = -\frac{\boldsymbol{a}}{\boldsymbol{a}_3}\frac{\boldsymbol{n}}{2}\left[\tanh\left(\frac{x-V_3 t}{\Delta_3}+\boldsymbol{d}\right)-\tanh\left(\frac{x-V_3 t}{\Delta_3}-\boldsymbol{d}\right)\right] \tag{31}$$

Here $\boldsymbol{n}$ is a free parameter measuring the degree of nonlinearity and ranges over (0, 1). The nonlinear speed V_3 and characteristic width Δ_3 are different from their KDV equivalents; and are given by: *[Ostrovsky and Stepanyants, 1989; Stanton and Ostrovsky, 1999]*

$$\boldsymbol{d}(\boldsymbol{n}) = \frac{1}{4}\ln\left(\frac{1+\boldsymbol{n}}{1-\boldsymbol{n}}\right), \qquad \Delta_3 = \sqrt{\frac{-24\boldsymbol{a}_3\boldsymbol{g}}{\boldsymbol{a}^2\boldsymbol{n}^2}}, \qquad V_3 = c_0 - \frac{\boldsymbol{a}^2\boldsymbol{n}^2}{6\boldsymbol{a}_3} \tag{32}$$

It is interesting that the maximum amplitude of the kink,

$$\boldsymbol{h}_0 = \frac{\boldsymbol{a}}{\boldsymbol{a}_3}\tanh(\boldsymbol{d}) \tag{33}$$

is limited to $\boldsymbol{a}/\boldsymbol{a}\,3$, i.e., there exists a theoretical limiting amplitude to solitons described by the modified KDV equation. A plot of the CombKDV waveform is shown on Fig. 2 for a number of values of $\boldsymbol{n}$ [*Stanton and Ostrovsky, 1999*].

Solitons in the ocean sometimes show evidence of small cubic nonlinearities in the leading pulse but rarely in the trailing smaller-amplitude oscillations. However, there are well-known exceptions in Knight Inlet, a fjord-like body in British Columbia, [*Farmer and Smith, 1978, 1980; Henyey and Hoering, 1997*], and in the Pacific Ocean off the Columbia River, Oregon [*Stanton and Ostrovsky,1999; Kropfli et al., 1999*]. These solitons are very strongly nonlinear and require the full theoretical apparatus of Eq. (29).

6. Summary

It has been nearly four decades since the first in-situ observations were made of nonsinusoidal waveshapes for internal waves on the continental shelf [*LaFond, 1962*]. However, it has only been since satellite images have been acquired in sufficient quantity that the global extent and the recurrency of the waves have been appreciated. In this regard, the accumulation of some ten years of SAR data from ERS-1/2 and Radarsat-1 has added greatly to the limited but tantalizing pictures from Landsat [*Sawyer and Apel, 1976*] and Seasat [*Fu and Holt, 1982*].

The case studies in the Atlas have helped to show the observed dominant characteristics of internal solitons in the ocean. They are:

- The solitons are ubiquitous in the ocean, appearing wherever the proper combination of density gradient, current flow, and bathymetry occur.
- The generation process launches undulatory internal bores on each semidiurnal tide, with significant modulations on diurnal, fortnightly, seasonal, and semiannual time scales.
- The solitons are produced via lee wave formation, shear flow instability, or scattering of barotropic modes into internal baroclinic modes at locales close to rapidly shoaling depths that protrude into the pycnocline. The exact mechanisms are not yet clear.
- They occur in packets, usually rank-ordered, with the largest, fastest, greatest-wavelength, and longest-crested oscillations appearing at the packet front, which then slowly decay to

An Atlas of Oceanic Internal Solitary Waves (May 2002)   **Oceanic Internal Waves and Solitons**
by Global Ocean Associates
Prepared for Office of Naval Research – Code 322 PO

smaller-amplitude, reduced-wavelength, and shorter-crested oscillations at the rear. The orientation of packet wavefronts in the horizontal plane is controlled by refraction and to a lesser extent in narrow straits, by diffraction.

- The solitons are the leading edge of an undulatory internal tidal bore generated by tidal flow over banks, sills, and continental shelf breaks. The distance between successive bores is the internal tidal wavelength on the continental shelf. As the packet approaches, each bore is characterized by a sharp drop in pycnocline depth approximately equal to the soliton amplitude, a sequence of nonlinear oscillations that decrease in amplitude from front to rear, and a slow recovery of the depression over several hours. Wavelengths are longest at the packet front and shortest at the rear. All wavelengths increase logarithmically as time goes on, due to the higher speeds of larger solitons.
- They are dissipated by radial spreading, bottom interactions, instability, and fluid turbulence. Lifetimes are the order of a few days in the open sea and a day or so on the shelf.

KDV theory, in the form of the quadratic KDV and the cubic combKDV equations, works surprisingly well to describe internal solitary waves in the sea when measured by its ability to simulate the local two-dimensional hydrodynamics of soliton packets. While nature is much more disorderly than mathematical theory, nevertheless internal solitons are among the most coherent and reproducible phenomena in the sea, barotropic astronomical tides perhaps excepted. Since tidal currents are one ingredient in the recipe for production of solitons (the others being stratification and variable bathymetry that perturbs the density structure), it is not surprising that solitons follow the tides and the seasons. Furthermore, their very coherency allows detailed comparisons between observation and models in a satisfying way.

The characterization of soliton packets as oscillations on the leading edge of the nonlinear internal tide is more recent [*Gerkema, 1994, 1996; Apel, 1998*]. Viewed from this perspective, the solitons can be regarded as part of the response of a fluid to an imposed internal shock, that is, they are a "ringing" of the leading edge of a super-Froude shock front moving across the ocean and repeated every 12 ½ hours. This front transports mass and momentum in both its mean and its fluctuations. The other part of the response lies in the recovery from the initial downward displacement of the density field during the remainder of the tidal cycle. The inclusion of Coriolis effects, which has not been mentioned here, has an inhibiting influence on the onset of oscillations [*Gerkema, 1994*]. Differences and similarities between solitons generated at shelf breaks and sills are pointed out, with the water depth in the far field being important to the lifetime of the waves. Packets generated at sills appear to be, on the average, more energetic than those at shelf breaks, and to take on more of the characteristics of solibores [*Henyey and Hoering, 1997*]; this is probably related to the intensity of tidal flows near sills. The exact mechanisms for generation are not yet established, but the two main hypotheses, lee-wave formation and barotroic–baroclinic scattering, seem to happen at various locales. Neither are the relative magnitudes of the various dissipation mechanisms known. This difficult problem is also a first-order research issue and important to resolve because of its impact on oceanic optical opacity, nutrification, and bio-stimulation.

An Atlas of Oceanic Internal Solitary Waves (May 2002)   **Oceanic Internal Waves and Solitons**
by Global Ocean Associates
Prepared for Office of Naval Research – Code 322 PO

7. References

Alpers, W., 1985: Theory of radar imaging of internal waves. Nature, 314, 245-247.

Alpers, W., Heng W.C., and Lim, H., 1997: Observation of internal waves in the Andaman Sea by ERS SAR, in Third ERS Symposium on Space at the Service of Our Environment, V. III, 1287-1291.

Apel J. R., 2003: A New Analytical Model for Internal Solitons in the Ocean, J. Physical Oceanography, 33 (11), 2247-2269

Apel, J. R., 2000: *Solitons near Gibralta*r: *Views from the European Remote Sensing Satellite*s, Global Ocean Associates, Silver Spring, MD. 23 pp.

Apel, J. R., 1999, "Amplification of internal waves by shear-flow instability: A new view and new possibilities," Report GOA 99-2, Global Ocean Associates, Silver Spring, MD, 20pp.

Apel, J. R., 1998: Comparisons between the dnoidal soliton model and observations, Proc.of PORSEC'98-Qingdao, Vol.1, 444-447, M.-X He and G. Chen, eds., PORSEC'98 Secretariat, Qingdao, China.

Apel, J. R., 1987: *Principles of Ocean Physic*s, Academic Press, Ltd., London, 634 pp

Apel, J. R., 1979: Observations of internal wave surface signatures in ASTP photographs, Apollo-Soyuz Test Project Summary Science Report, V. II, 505–509, El-Baz and Warner, (eds), NASA SP-12, NASA, Washington, DC.

Apel, J. R. and P. F. Worcester, 2000: "Internal solitons near Gibraltar: A longitudinal study using ERS-1 and 2 SAR imagery," in Proc. ERS–Envisat Symposium: Looking Down to Earth in the New Millennium, European Space Agency, ESRIN/Publications.

Apel, J.R., Baidey, M, Chiu, C.-S., Finette, S., Headrick, R., Kemp, J., Neuhall, A., Orr, M. H., Pasewark, B., Tielbuerger, D., Turgut, A., Von Der Heydt, K., Wolf, S., 1997, An Overview of the 1995 SWARM Shallow-Water Internal Wave Acoustic Scattering Experiment, IEEE J. Oceanic Eng., vol. 22, pg. 465-500.

Apel, J.R., J.R. Holbrook, J. Tsai, and A.K. Liu, 1985: The Sulu Sea internal soliton experiment. J. Phys. Oceanogr., 15 (12), 1625-1651.

Apel, J. R., and J. R. Holbrook, 1983: Internal solitary waves in the Sulu Sea, Johns Hopkins APL Tech. Digest 4, No.4, 267-275.

Apel, J.R., and F.I. Gonzalez, 1983: Nonlinear features of internal waves off Baja California as observed from the SEASAT Imaging Radar. *J. Geophys. Re*s., **88 (C7**), 4459-4466.

Apel, J.R., J.R. Proni, H.M. Byrne, and R.L. Sellers, 1975a: Near-simultaneous observations of intermittent internal waves on the continental shelf from ship and aircraft. Geophys. Res. Lett., 2, 128-131.

Apel, J.R., H.M. Byrne, J.R. Proni, and R.L. Charnell, 1975b: Observations of oceanic internal and surface waves from the Earth Resources Technology Satellite. J. Geophys. Res., 80 (6), 865-881.

An Atlas of Oceanic Internal Solitary Waves (May 2002)   **Oceanic Internal Waves and Solitons**
by Global Ocean Associates
Prepared for Office of Naval Research – Code 322 PO

Armi, L., and D.M. Farmer, 1988: The flow of Mediterranean water through the Strait of Gibraltar. Progress in Oceanography, 21 (1), 1-105.

Benjamin, T. B., 1962, "The solitary wave on a stream with an arbitrary distribu-tion of vorticity," J. Fluid.Mech.12: 97-116.

Benjamin, T. B., 1966, "Internal waves of finite amplitude and permanent form," J. Fluid Mech. 25, part 2, 241-270.

Benny, D. J., 1966, "Long non-linear waves in fluid flows, " J. Math. Phys., 45, 52—63.

Booker, J. R. and F. B. Bretherton, 1967, "The critical layer for internal gravity waves in a shear flow," J. Fluid. Mech. 27, 513-539.

Dodd, R. K., J. C. Eilbeck, J. D. Gibbon, and H. C. Morris, 1982, Solitons and Nonlinear Wave Equations, Academic Press, Ltd., London.

Ekman, V. W., 1904, "On dead water," *Sc*i. *Result*s. *Nor*w. *North Polar Exped*i. 1893–96, 5, 15.

Ewing, G., 1950, Slicks, surface films and internal waves, *J. Mar. Res.*, 9, 161,

Farmer, D., and L. Armi, 1999: The generation and trapping of solitary waves over topography. *Scienc*e, **28**3, 188-190.

Farmer, D.M., and L. Armi, 1988: The flow of Atlantic water through the Strait of Gibraltar. Progress in Oceanography., 21 (1), 1-105.

Farmer, D.M., and J.D. Smith, 1978, "Nonlinear waves in a fjord," in Hydrody-namics of Estuaries and Fjords, ed. by J.C.H. Nihoul, Elsevier Scientific Publishing Company, 465-493.

Farmer, D.M., and J.D. Smith, 1980, "Tidal interaction of stratified flow with a sill in Knight Inlet," Deep-Sea Res., 27A, 239-254.

Fu, L.L., and B. Holt, 1982, Seasat Views Oceans and Sea Ice with Synthetic Aperture Radar, JPL Publication 81-120, Pasadena CA, 200pp.

Gargett, A.E., and B.A. Hughes, 1972, On the interaction of surface and internal waves, *J. Fluid Mech.*, 52, 179-191.

Gurevich, A. V., and L. P. Pitaevskii, 1973a, "Nonstationary structure of a collisionless shock wave," ZhETF, 65, N.2, 590—595 (in Russian). (Engl. transl.: 1974, Sov. Phys. JETP, 38, 291 -297.)

Gurevich, A. V., and L. P. Pitaevskii, 1973b, "Decay of Initial Discontinuity in the Korteweg-De Vries Equation," JETPLett.V,17,No.5, 193-195.

Gurevich, A. V., A. L. Krylov, and G. A.'El', 1990, "Nonlinear modulated waves in dispersive hydrodynamics," Sov. Phys. JETP 71, (5), 899-910.

Grimshaw, R., 1981, "Evolution equations for long nonlinear waves in stratified shear flows," Stud. Appl. Math., 65, 159—188.

Grimshaw, R., L.A. Ostrovsky, V.I. Shrira, and Yu. A. Stepanyants, 1998, "Long nonlinear surface and internal gravity waves in a rotating ocean," Surveys in Geo-physics, 19, 289-338.

An Atlas of Oceanic Internal Solitary Waves (May 2002)   **Oceanic Internal Waves and Solitons**
by Global Ocean Associates
Prepared for Office of Naval Research – Code 322 PO

Halpern, D., 1970: Semidiurnal tides in Massachusetts Bay. J. Geophys. Res., 76, 6573-6584.

Halpern, D., 1971: Observations of short period internal waves in Massachusetts Bay. J. Mar. Res., 29, 116-132.

Haury, L.R., M.G. Briscoe and M.H. Orr, 1979, "Tidally generated internal wave packets in Massachusetts Bay," Nature, 278 (5702), 312-317.

Henyey, F. S. and A. Hoering, 1997, Energetics of borelike internal waves, J. Geophys. Res. 102, 3323-3330.

Hsu, M.-K., A.K. Liu, and C. Liu, 2000a: A study of internal waves in the China Seas and Yellow Sea using SAR. Continental Shelf Res., 20, 389-410.

Hsu, M.-K., and A.K. Liu, 2000b: Nonlinear internal waves in the South China Sea. Canadian J. Rem. Sens. 26, no.2, 72-81.

Hughes, B.A., and J.F.R. Gower, 1983, SAR imagery and surface truth comparisons of internal waves in Georgia Strait, British Columbia. J. Geophys. Res., 88 (C3), 1809-1824.

Joseph, R. J., 1977, "Solitary waves in a finite depth fluid," J.Phys.A:Math.and Gen., 10, N.12, L225—L227.

Kao, T.W, Pan F-S, and D. Renouard, 1985, " Internal solitons on the pycnocline: generation, propagation and shoaling and breaking over a slope," J. Fluid Mech. 159, 19-53.

Keulegan, G.H., and L.H. Carpenter, 1961: An experimental study of internal progressive oscillatory waves. *Nat. Bur. Stand. Rep*t., 7319.

Kubota, T., D. R. S. Ko, and L. Dobbs, 1978, "Propagation of weakly nonlinear internal waves in a stratified fluid of finite depth," J. Hydronaut., 12, 157—165.

Koop, C.C., and G. Butler, 1981, "An investigation of internal solitary waves in a two-fluid system," J. Fluid Mech., 112, 225-251.

Korteweg, D. J., and G. de Vries, 1895, "On the change of form of long waves advancing in a rectangular canal, and on a new type of long stationary wave," Phil. Mag., 39, Ser. 5, 422—443.

Kropfli, R.A., L.A. Ostrovsky, T.P. Stanton, E.A. Skirta, A.N. Keane, and V.A. Irisov, 1999: Relationships between strong internal waves in the coastal zone and their radar and radiometric signatures. *J. Geophys. Re*s., 104 (C2), 3133-3148.

Lafond, E.C., 1962: Internal waves, Part I. The Sea, ed. by M.N. Hill, Wiley-Interscience, New York, 731-751.

Lee, Ch-Y. and R. C. Beardsley, 1974. "The generation of long nonlinear internal waves in a weakly stratified shear flow," J. Geophys. Res. 79, 453-457.

Levine, M.D., L. Padman, R.D. Muench and J.H. Morison, 1997, Internal waves and ties in the western Weddell Sea: Observations from Ice Station Weddell, J. Geophys. Res. 102, 1073-1089.

Lindzen, R. S., 1988, "Instability of plane parallel shear flow (Toward a mechanistic picture of how it works)," PAGEOPH 126, 103-121.

38

An Atlas of Oceanic Internal Solitary Waves (May 2002) **Oceanic Internal Waves and Solitons**
by Global Ocean Associates
Prepared for Office of Naval Research – Code 322 PO

Liu, A.K., J.R. Holbrook, and J.R. Apel, 1985, "Nonlinear internal wave evolution in the Sulu Sea," J. Phys. Oceanogr.15 (12), 1613-1624.

Liu, A. K., and D. J. Benny, 1981, "The evolution of nonlinear wave trains in stratified shear flows," Stud. Appl. Math.64, 247-269.

Maxworthy, T., 1979: A note on the internal solitary waves produced by tidal flow over a three-dimensional ridge. J. Geophys. Res. 84, 338-346.

Maslowe, S.A., and L.G. Redekoop, 1980, Long nonlinear waves in stratified shear flows, *J. Fluid Mech*., 101, Pt. 2, 321-348.

Orr, W. M. F., 1907, "The stability or instability of the steady motions of a perfect liquid and a viscous liquid," Proc. Roy. Irish Acad. A27, 9-138.

Osborne, A. R., 1995, "Solitons in the periodic Korteweg-de Vries equation, the Θ-function representation, and the analysis of nonlinear, stochastic wave trains," Phys. Rev. E, 52, 1105-1122.

Osborne, A.R., and T.L. Burch, 1980: Internal solitons in the Andaman Sea. Science, 208 (4443), 451-460.

Ostrovsky, L. A., 1978, "Nonlinear internal waves in a rotating ocean," Okean-ologia, 18, 181—191 (in Russian). (Engl. transl.: Oceanology 18, N.2, 119—125.)

Ostrovsky, L.A., and Y.A. Stepanyants, 1989, "Do internal solitons exist in the ocean?" Rev. of Geophys., 27(3), 293-310.

Pinkel, R., M. Merrifield, M. McPhaden, J. Picaut, S. Rutledge, D. Siegel, and L. Washburn, 1997: Solitary waves in the western Equatorial Pacific Ocean. Geophys. Res. Lett., 24 (13), 1603.

Rocklift, N., 1984, "Long nonlinear waves in stratified shear flows," Geophys. and Astrophys. Fluid Dynamics 28, 55-75.

Russell, J. S., 1838, "Report to committee on waves," Reportofthe 7thMeeting of British Association for the Advancement of Science, London, John Murray, 417—496.

Russell, J. S., 1844, "Report on waves," Report of the 14th Meeting of British Association for the Advancement of Science., London, John Murray, 311—390.

Sandstrom, H., and J.A. Elliot, 1984, "Internal tide and solitons on the Scotian Shelf: A nutrient pump at work," J. Geophys. Res., 89 (C4), 6415-6426.

Sawyer, C. and J. R. Apel, 1976: Satellite images of oceanic internal wave signatures, National Oceanic & Atmospheric Administration, Environmental Research Laboratories, NOAA S/T 2401.

Segur, H., and J. L. Hammack, 1982, "Soliton models of long internal waves," J. Fluid Mech., 118, 285—304.

Shand, J.A., 1953, Internal waves in the Georgia Strait, *Eos. Trans. AGU*, 34, 849-856.

An Atlas of Oceanic Internal Solitary Waves (May 2002)   **Oceanic Internal Waves and Solitons**
by Global Ocean Associates
Prepared for Office of Naval Research – Code 322 PO

Suvorov, A. M., 1981, "Evolution of quasi-plane weakly nonlinear internal waves in a viscous fluid," Izv. AN SSSR. Mekhanika Zhidkosti i Gaza, 16, N.6, 158—162 (in Russian). (Engl. transl.: 1982, Fluid Dynamics, 16, N.6, 934—937.)

Wallace, A. R., 1869, 1922, The Malay Archipelago, Dover Publications, New York, 370–374, 410–413.

Wesson, A. C. and M. C. Gregg, 1988, "Turbulent dissipation in the Strait of Gibraltar and associated mixing," in Small-Scale Turbulence and Mixing in the Ocean, eds. J.C.J. Nihoul and B. M. Jamar, Elsevier, Amsterdam. 541 pp.

40

An Atlas of Oceanic Internal Solitary Waves (May 2002)   **Oceanic Internal Waves and Solitons**
by Global Ocean Associates
Prepared for Office of Naval Research – Code 322 PO